NAZARBAYEV
UNIVERSITY

APPLICATION OF SPECTRAL FLOW CYTOMETRY FOR CHARACTERIZATION OF ALGAL AND MICROBIAL PHENOTYPES

DAMIR USSIBALIYEV
(B.Sc., Nazarbayev University)

A THESIS SUBMITTED
FOR THE BIOL491 Honor Thesis
DEPARTMENT OF BIOLOGY
SCHOOL OF SCIENCES AND HUMANITIES
NAZARBAYEV UNIVERSITY
2025

PRINCIPAL INVESTIGATOR: DR. NATALIE BARTENEVA

DECLARATION

I hereby declare that the thesis is my original work and it has been written by me in its entirety. I have duly acknowledged all the sources of information which have been used in the thesis. This thesis has also not been submitted for any degree in any university previously.

Damir Ussibaliyev

(*Student's name*)

25 April 2025

ACKNOWLEDGEMENTS

Special thanks to Natalie Barteneva (Nazarbayev University), Ayagoz Meirkhanova, Aizada Bexeitova and Polina Len (Department Biology, Nazarbayev University) for the guidance, technical expertise and supervision, as well as providing informational support and editorial assistance with the research project.

Additional thanks for Sabina Marks (CCAC, University of Duisburg-Essen) for consultation regarding algae cultivation and perpetuation of algae cultures.

TABLE OF CONTENTS

Nazarbayev University, School of Science and Humanities, Department of Biology
Bachelor's Degree Program in Biology
Damir Ussibaliyev: Application of Spectral Flow Cytometry for Characterization of Algal and Microbial Phenotypes
BIOL 491 thesis; xx pages, x appendix(es) (12pt)
Supervisor: Natalie Barteneva, MD, PhD, Department of Biology
25.04.2025
Keywords: algae, phenotyping, pigments, spectral flow cytometry, chlamidomonodales

SUMMARY

Microalgae and bacteria play a crucial role in aquatic ecosystems and hold significant potential for biotechnological applications. Traditional flow cytometry (FC) faces challenges in analyzing microalgae due to interference from pigments and secondary metabolites. This study leverages spectral flow cytometry to overcome these limitations, allowing for high-resolution, label-free characterization of phenotypes of microscopic organisms by capturing full-spectrum autofluorescence signals. Focusing on one bacterial specie (*Serratia marcescens)* and four algae species of the Chlamydomonadales order (*Chlamydomonas reinhardtii*, *Gonium pectorale*, *Chlorococcum sp.*, and *Pandorina morum*), we investigated how growth phases and cellular morphology influence spectral signatures. Our results revealed distinct subpopulations within cultures, identifiable by variations in chlorophyll autofluorescence as well as accessory pigment autofluorescence. Key findings include the correlation of accessory pigment fluorescence with growth dynamics, while chlorophyll autofluorescence combined with fluorescence of metabolic pigments distinguished viable, dying, and dead cells. Additionally, spectral variance analysis highlighted metabolic shifts during growth, demonstrating the dynamic nature of pigments in the organisms over their growth cycle. This work proposes a novel method for monitoring algal cultures in biotechnological processes using accessory pigment spectra and demonstrates the utility of spectral flow cytometry to identify and distinguish spectral phenotypes of microscopic organisms.

LIST OF TABLES

LIST OF FIGURES AND ILLUSTRATIONS

ABBREVIATIONS

FSC – forward scatter

SSC – side scatter

ODU – optical density units

nm - nanometers

CH – channel (of detection)

CV –coefficient of variance

1. Introduction

1.1 Background and Literature Review

1.1.1 Ecological Importance of Algae and Bacteria Phenotyping

Algae and bacteria are key players in biogeochemical cycles, contributing to carbon fixation, nitrogen cycling, and oxygen production. Phenotyping these microorganisms enables researchers to understand their adaptive strategies and functional roles in diverse ecosystems. For instance, cyanobacteria are responsible for approximately 50% of global photosynthesis (Field et al., 1998). Phenotypic traits such as pigment composition, growth rates, and nutrient uptake efficiency are critical for assessing their responses to environmental stressors like climate change and eutrophication (Falkowski & Raven, 2013). Similarly, bacteria exhibit remarkable phenotypic plasticity, allowing them to thrive in extreme environments, from deep-sea hydrothermal vents to arid soils (Fierer et al., 2012). Phenotyping bacterial communities helps to determine their roles in nutrient cycling and ecosystem resilience (Bardgett & van der Putten, 2014).

Phenotyping also aids in monitoring and mitigating harmful algal blooms (HABs) and bacterial pathogens in aquatic systems. HABs, often caused by cyanobacteria, produce toxins that threaten aquatic life and human health (Paerl & Paul, 2012). Phenotypic characterization of bloom-forming species, such as *Microcystis spp.*, provides insights into their toxin production mechanisms and environmental triggers (Harke et al., 2016). The health implications of algae and bacteria phenotyping are equally profound. Algae, particularly microalgae, are rich sources of bioactive compounds with antioxidant, anti-inflammatory, and antimicrobial properties (Guedes et al., 2011). Phenotyping these species for bioactive compound production and biocompatibility is crucial for advancing algal biotechnology.

In the context of bacteria, phenotyping is invaluable for understanding microbial pathogenesis and antibiotic resistance. Bacteria, such as *Escherichia coli* and *Staphylococcus aureus*, exhibit diverse phenotypic traits that influence their virulence and resistance profiles (Levin-Reisman et al., 2017) and, therefore, phenotyping these pathogens enables the identification of resistance mechanisms and the development of targeted therapies (Blair et al., 2015).

1.1.2 Autofluorescent Molecules

Chlorophyll, the primary pigment in photosynthetic microorganisms such as algae and cyanobacteria, is a well-known source of autofluorescence. It absorbs light in the blue and red

spectral regions and emits fluorescence in the red and far-red wavelengths. The study by Blankenship (2014) in "Molecular Mechanisms of Photosynthesis" provides detailed absorption and emission wavelength profiles for chlorophyll, emphasizing its role in assessing photosynthetic efficiency and cellular health.

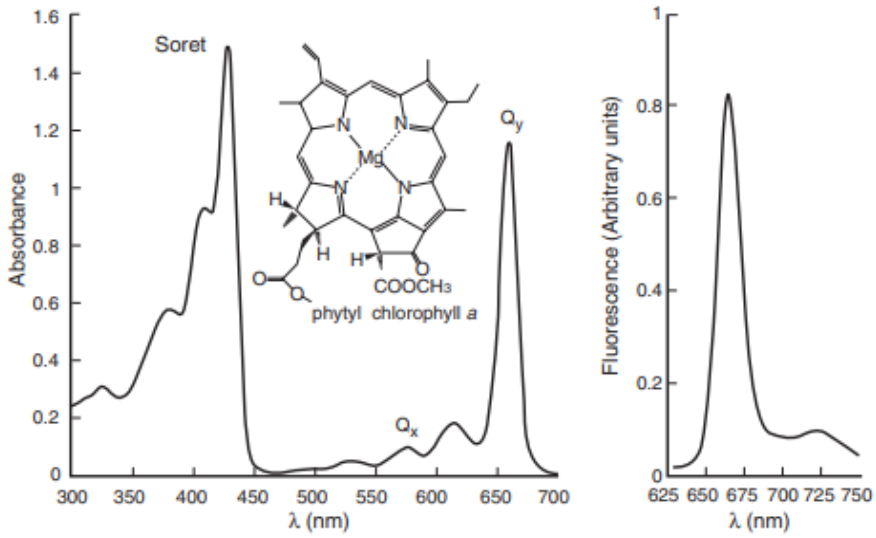

Figure 1. Absorption (left) and fluorescence emission (right) spectra of chlorophyll *a* in diethyl ether (adapted from Blankenship, 2014).

Chlorophyll fluorescence is widely used in flow cytometry and spectroscopic analysis to monitor the photosynthetic activity of algae both in natural and laboratory conditions. Environmental factors such as light intensity, nutrient availability, and temperature influence the quantum yield of chlorophyll fluorescence, making it a sensitive indicator of stress responses. For instance, under high-light conditions or nutrient deprivation, non-photochemical quenching mechanisms alter fluorescence intensity, providing insights into the physiological state of cells (Baker, 2008). This capability is particularly valuable in ecological studies, where chlorophyll fluorescence is used to monitor phytoplankton dynamics and assess water quality (Behrenfeld et al., 2009).

Carotenoids are another class of pigments in photosynthetic microorganisms that contribute to autofluorescence and play a dual role in light harvesting and photoprotection. These pigments absorb light in the blue-green spectrum and emit fluorescence in the green to orange range. Carotenoid fluorescence is particularly useful in assessing oxidative stress and photoinhibition in microalgae (Guedes et al., 2011).

Non-photosynthetic microorganisms also exhibit autofluorescence due to secondary metabolites such as non-photosynthetic pigments, flavins, and phenazines. Prodigiosin, a red non-photosynthetic pigment produced by *Serratia marcescens*, in the study by Andreyeva & Ogorodnikova (2015) on the spectral properties of prodigiosin, highlights its utility in microbial identification and metabolic studies.

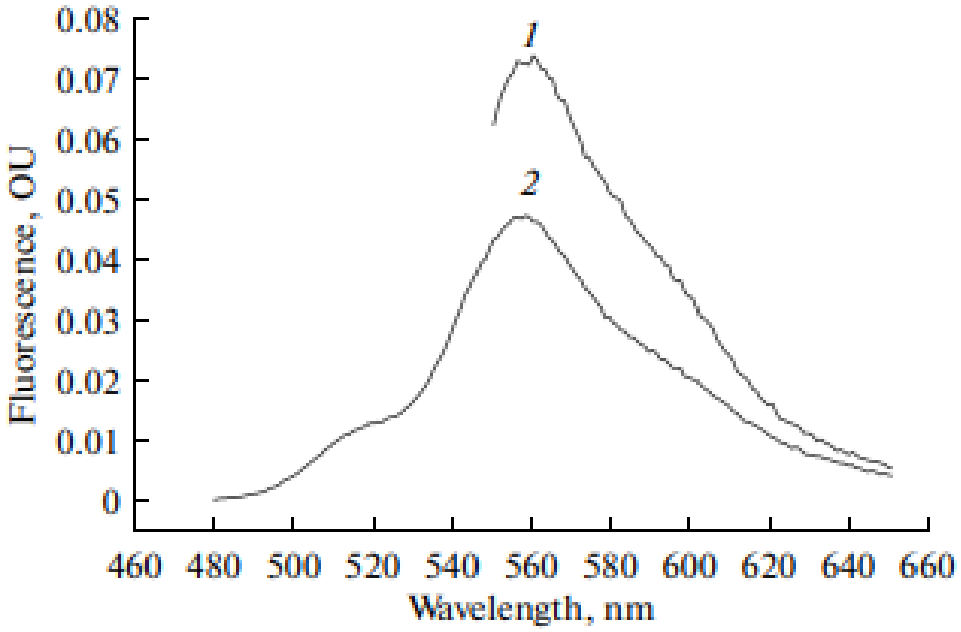

Figure 2. Prodigiosin fluorescence (ethanol solution): the "red" form (pH 4), excitation at 535 nm (1) and the "yellow" form (pH 10), excitation at 465 nm (2) (adapted from Andreyeva & Ogorodnikova, 2015).

Flavins, including riboflavin and flavin mononucleotide, fluoresce in the blue-green range and are involved in redox reactions (Murkharjee, 2013). These natural fluorophores are valuable tools for studying microbial interactions and adaptation strategies in diverse environments.

NADH fluorescence is a key indicator of cellular metabolism, with the reduced form (NADH) fluorescing in the blue-green region upon excitation in the UV-blue range. Variations in NADH fluorescence intensity and lifetime provide insights into metabolic shifts, such as transitions between glycolysis and oxidative phosphorylation (Lakowicz, 2006). This property makes NADH autofluorescence a valuable tool in studying metabolic responses of the cells to changes in the environment (Heidelman et al., 2021). Additionally, other cellular molecules, such as elastin, collagen, and lipopigments, contribute to autofluorescence. Lipofuscin, for

example, accumulates due to oxidative stress and aging, fluorescing in the yellow-to-red spectrum. These molecules serve as crucial markers in biomedical imaging and diagnostic applications, providing insights into cell health and pathological conditions (Croce & Bottiroli, 2014).

Table 1: Endogenous fluorophores recurrently exploited as intrinsic biomarkers in autofluorescence studies (adapted from Croce & Bottiroli, 2014).

Endogenous fluorophores	**Biological constituents**	**Autofluorescence (excitation) / (emission) ranges**	**Autofluorescence photophysical fingerprints and possible correlated alterations**
Aromatic amino acids: Phe, Tyr, Trp	Functional proteins	(240-280 nm) / (280-350 nm)	Spectral shape and amplitude (near UV, blue region tail)
Cytokeratins	Intracellular fibrous proteins	(280-325 nm) / (495-525 nm)	Spectral shape and emission amplitude
Collagen/Elastin	Extracellular fibrous proteins	(330-340 nm) / (400-410 nm) (350-420 nm) / (420-510 nm)	Excitation light birefringence effects spectral shape and emission amplitude, depending on maturation degree in eldering and fibrosis
NAD(P)H	Coenzymes of key enzymes in redox reactions	(330-380 nm) / (440, 462 nm, bound, free)	Spectral shape, emission amplitude
Flavins	Coenzymes of key enzymes in redox reactions	(350-370;440-450 nm) / (480/540 nm)	(NAD(P)Hbound/free, NAD(P)Htotal/oxidized $_{flavins}$ ratios, depending on aerobic/anaerobic energetic

			metabolism, antioxidant defense, inflammation, carcinogenesis
Fatty acids	Accumulated lipids	(330-350 nm) / (470-480 nm)	Spectral shape, emission amplitude and photosensitivity, depending on altered lipid metabolism
Primary carotenoids	Retinols and carotenoids	(370-380 nm) / (490-510 nm)	Spectral shape, emission amplitude and photosensitivity, depending on multiple functions including antioxidant and vision roles, and altered retinol metabolism
Protoporphyrin IX and porphyrin derivatives	Protein prosthetic group	(405 nm) / (630-700 nm)	Spectral shape, emission amplitude and photosensitivity, depending on heme and iron altered metabolism
Lipofuscins/Lipofuscin like-lipopigments/ceroids	Miscellaneous (proteins, lipids, retinoids)	(UV, 400-500 nm) / (480-700 nm)	Spectral shape, emission amplitude depending on eldering, oxidation degree, cell stemness degree

1.2.3 Spectral Flow Cytometry and Its Advantages over Conventional Techniques

Flow cytometry has revolutionized bacterial and microalgal research by enabling rapid assessment of cell density, viability, and fluorophore composition. Chlorophyll autofluorescence is a key parameter in flow cytometric analysis, allowing for non-invasive

monitoring of algal growth and physiological status (Dubelaar et al., 1999). Multi-parametric flow cytometry further enables differentiating microalgal species based on accessory pigments such as phycoerythrin and phycocyanin, aiding in biodiversity studies and environmental assessments (Sosik et al., 2010). Flow cytometry is also instrumental in monitoring microalgal stress responses. Shifts in fluorescence intensity and cellular morphology provide insights into the health and adaptability of microalgal cultures, optimizing cultivation conditions for biofuel production and wastewater treatment (Juneau et al., 2015). It is already widely used to quantify natural planktonic bacterial communities and assess bacterial abundance and diversity in aquatic environments (Marie et al., 1997). Nucleic acid stains such as SYBR Green and propidium iodide enable the distinction between live and dead bacterial cells, enhancing microbial population assessments (Berney et al., 2007). Additionally, flow cytometry is used to study bacterial resistance mechanisms, providing rapid antibiotic susceptibility testing for clinical applications (Suller & Lloyd, 1999). Flow cytometry offers several advantages over traditional methods such as microscopy and culture-based techniques. It provides high-throughput, automated analysis with improved statistical power, overcoming the limitations of microscopy and the bias of culture-based methods (Davey & Kell, 1996). The study by Sieracki et al. (1999) highlights the superiority of flow cytometry in detecting microbial contaminants in ballast water, demonstrating its efficiency in environmental microbiology.

Spectral flow cytometry is a natural development of conventional flow cytometry that allows for deeper analysis of the emission spectra of the samples without sacrificing advantages of the conventional flow cytometry over traditional techniques. Spectral flow cytometry enables high-resolution analysis of complex microbial communities, while single-cell sequencing links phenotypic traits with genetic information (Nolan & Condello, 2013). The development of spectral imaging cytometry, as detailed in “Spectral and Imaging Cytometry” (Barteneva, Vorobyev, 2023), represents a significant leap forward in cellular phenotype differentiation. By capturing both spectral and spatial data, this technique provides a more comprehensive understanding of phenotypes’ differences based on their multicolor panels and autofluorescence as separate parameters.

The phenotyping of algae and bacteria, combined with autofluorescence and spectral flow cytometry, is a vital scientific endeavor with far-reaching ecological implications. These techniques provide rapid, non-invasive, and high-resolution analysis of microbial and algal populations, enabling advancements in environmental monitoring, industrial biotechnology, and medical diagnostics. Despite these advances, critical gaps in the understanding of the

observed phenotypic heterogeneity and their importance to ecological function and adaptations are still present. Most studies overlook temporal changes in the composition of the populations and phenotypic dynamics within these populations. This study aims to fill that gap in knowledge by integrating spectral flow cytometry with conventional microbiological methods (optical density), offering a system-level perspective on the phenotype dynamics of microscopic organisms.

1.2 Research Question

How algal growth and changes in cellular and cluster morphology of Chlamydomonadales order algae affect algal spectral parameters.

1.3 Hypothesis

We hypothesize that full-spectrum phenotyping signatures of microalgae are associated with major and accessory algal pigments as well as secondary metabolites during different stages of cell growth.

2. Materials and Methods

2.1 Bacterial Cultures

Serratia marcescens (ATCC 4003)

2.2 Algae Cultures

Chlamydomonas reinhardtii (ATCC 18798)

Gonium pectorale (CCAC 0085)

Chlorococcum sp. (CCAC 1330)

Pandorina morum (CCAC 0063)

2.3 Bacteria Cultivation

Bacterial cultures were obtained from the American Type Culture Collection (ATCC).

Samples were stored at 4°C between experiments. Samples were grown on solid Nutrient Agar (Thermo Fisher Scientific, USA) medium for 15 hours at 30°C in MaxQ™ 4000 Benchtop Orbital Shaker (Thermo Fisher Scientific, USA). The inoculation is performed in sterile conditions in the EuroClone SafeMate 1.5 Class II laminar flow cabinet (EuroClone, Italy).

2.4 Algae Cultivation

Algal samples were obtained from the Central Collection of Algal Cultures (CCAC) of the University of Duisburg-Essen (UDE). Samples were grown in 40ml tissue culture flasks with stocks maintained at 15ml of Warris-H (UDE, Germany) medium, maintained under dim light conditions, with a 12/12 hours day/night cycle at 22.5°C. Every 4 weeks 1.5ml of stock sample is transferred to 13.5ml of fresh Warris-H medium and grown under bright light conditions for 7 days, then transferred to the dim light rack. The transfer is performed in sterile conditions in the EuroClone SafeMate 1.5 Class II laminar flow cabinet (EuroClone, Italy).

2.5 Optical Density Readings

The optical density of the algal species was performed on a Thermo Scientific Varioscan (Thermo Fisher Scientific, USA) plate reader at 600nm and 750 nm wavelengths. Readings were obtained for the initial stock sample and every 24h interval during the 12-day growth cycle. Fresh Warris-H medium was used as a blank sample for each reading. The obtained data was analyzed and plotted using Microsoft Excel (Microsoft, USA).

2.6 Full-Spectrum Cytometry Analysis

Algae and bacterial samples were recorded using ID7000 Spectral Cell Analyzer (Sony Biotechnology, USA). Recordings were performed in conjunction with the Optical Density readings. 320, 355, 405, 488, 561, 637, and 808nm lasers were used to obtain full spectrum readings.

Samples were further analyzed using the in-built ID7000 Autofluorescence Finder Tool vs.2.0.2 software tool (Sony Biotechnology, USA) to visualize and perform gating on the distinct populations present in the samples. Subpopulations were identified based on the separation of the distinct population clusters and gated with optimized virtual filters (VFs) to obtain the data specific to each subpopulation as described before (Barteneva et al., 2019).

2.7 Analysis of the Changes in Algal Signatures

The longitudinal data collected throughout the growth cycle of the algae species was analyzed for the changes in the spectral shapes using coefficient of variation (CV) analysis.

Overlay data from the ID7000 instrument (Sony Biotechnology, USA) was collected and used to generate the table of the values for each laser and its corresponding detection channels. Data for each laser was arranged longitudinally. Coefficient of variation (Standard deviation of the population/mean) was calculated for each detected wavelength and used to generate line graph for better representation using Microsoft Excel (Microsoft, USA).

3. Aims of the Thesis Project

i. Develop stable cultures of algae *C.reinhardtii, G.pectorale, Chlorococcum sp., P.morum* (Chlamydomonadales order) from Central Collection of Algal Cultures (CCAC) (Germany, Duisburg- Essen University).

ii. Achieve stable growth between transfers during the experiment.

iii. Apply full-spectrum cytometry to characterize spectral phenotypes of the researched species.

4. Results

4.1 Growth Measurements through Optical Density

To observe the changes in the growth of the organisms Optical Density for 600nm and 750nm wavelengths was measured for algal samples. Figure 3 shows the changes observed throughout the growth cycles of the algal samples.

A

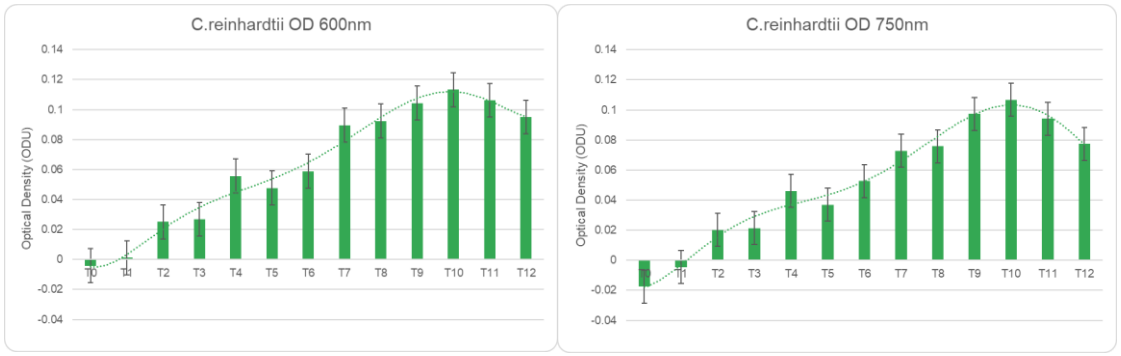

B

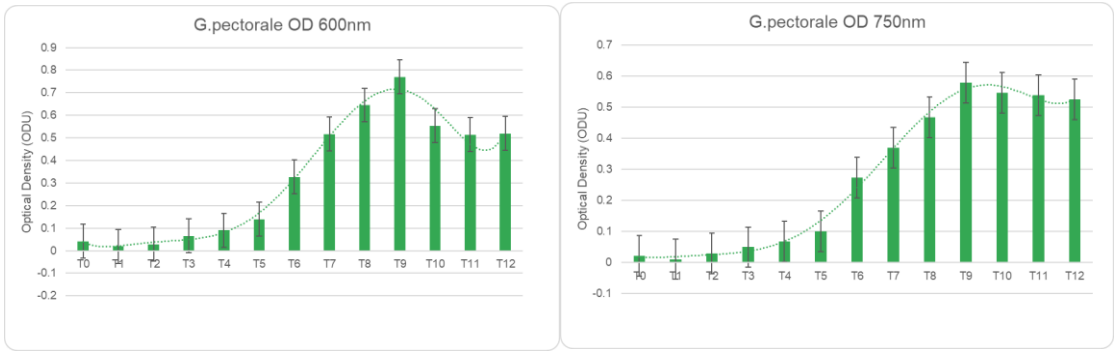

C

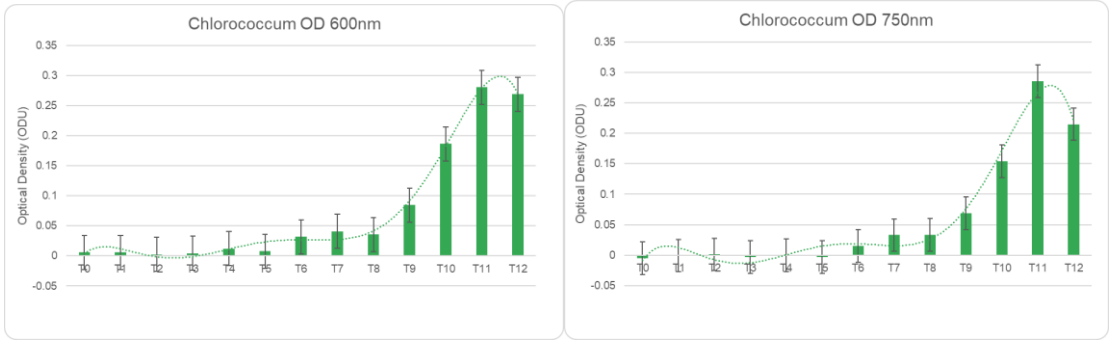

D

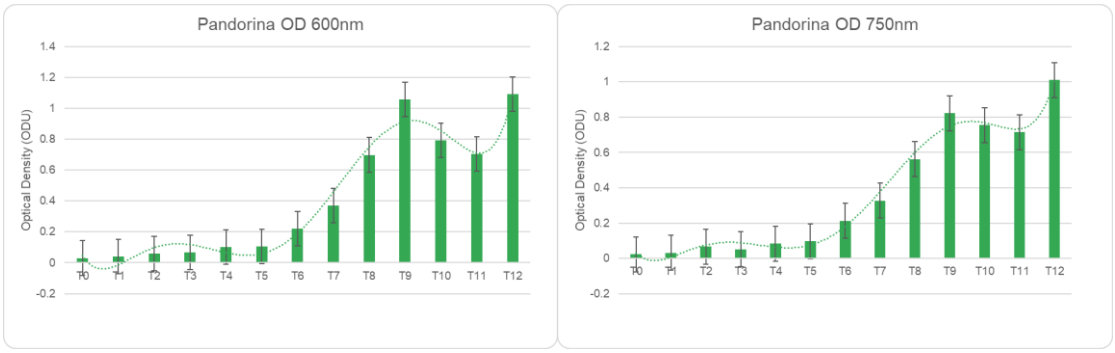

Figure 3. Values of the Optical Density readings at 600nm (OD600) and 750nm (OD750) wavelength. OD600 is used to evaluate the total biomass of the sample and OD750 is used to determine the total amount of chlorophyll in the sample. **A**. Optical density of the *C.reinhardtii* sample recorded over a 12-day growth cycle using 600nm (left) and 750nm (right). **B**. Optical density of the *G.pectorale* sample recorded over a 12-day growth cycle using 600nm (left) and 750nm (right). **C**. Optical density of the *Chlorococcum sp.* sample recorded over a 12-day growth cycle using 600nm (left) and 750nm (right). **D**. Optical density of the *P.morum* sample recorded over a 12-day growth cycle using 600nm (left) and 750nm (right).

The data obtained through optical density assays demonstrate the dynamics of the algae growth, with the OD600 showing a general increase in the biomass in the samples and the OD750 demonstrating an increase in the amount of chlorophylls present in the samples.

4.2 Autofluorescence-Based Discrimination of Microbial and Algal Subpopulations

Autofluorescence was later then utilized to discriminate the populations based on the intrinsic autofluorescence differences of the cells in different stages of growth. By using the "Autofluorescence Finder" tool, autofluorescence populations were found across all lasers. Autofluorescence signatures present in samples allow us to predict the minimal number of possible populations present in the sample at each recorded time point. Individual spectral signatures of each population are then extractable and ready to be analyzed. Figure 4 represents the usual workflow that was applied throughout the experiment to abstain separate fingerprints for each recorded sample.

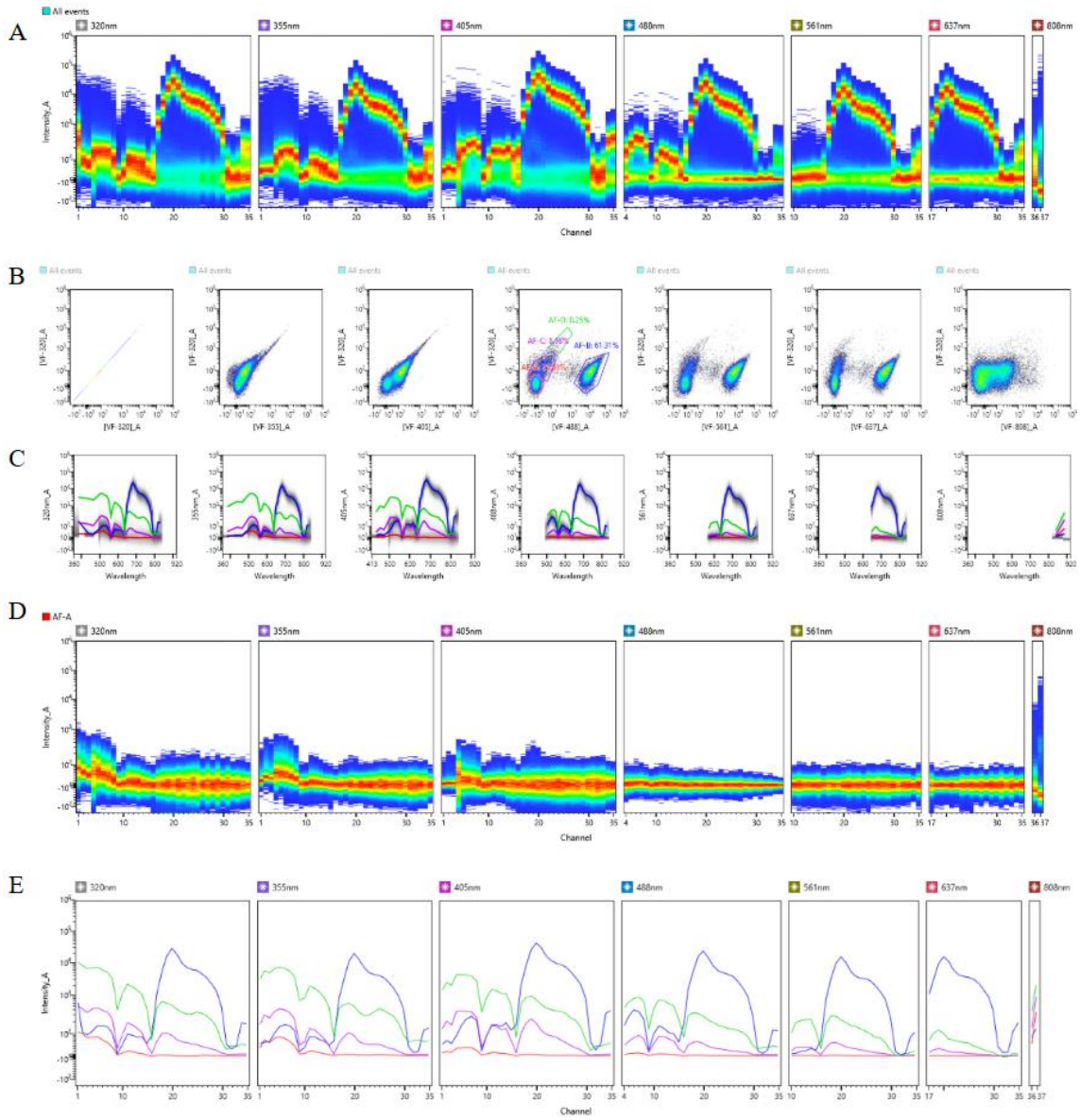

Figure 4. Experimental workflow for the spectral unmixing based on the autofluorescence patterns using ID7000 spectral flow cytometer (Sony Biotechnologies, USA). **A.** Recording of the single autofluorescence signature of the sample. **B.** Isolation of distinct phenotypes based on the optimal Virtual Filters setup. **C.** Respective emission spectra of the identified phenotypes. **D.** Ribbon plot representation of the identified phenotype. **E.** Overlay plot of the library of respective autofluorescence signatures of the identified phenotypes.

4.2.1 Bacterial Full-Spectrum analysis

Serratia marcescens

Main differences that occur during the growth cycle of the *S.marcescens* is the development of prodigiosin, which generates a distinct phenotype in the sample after 9 hours of growth.

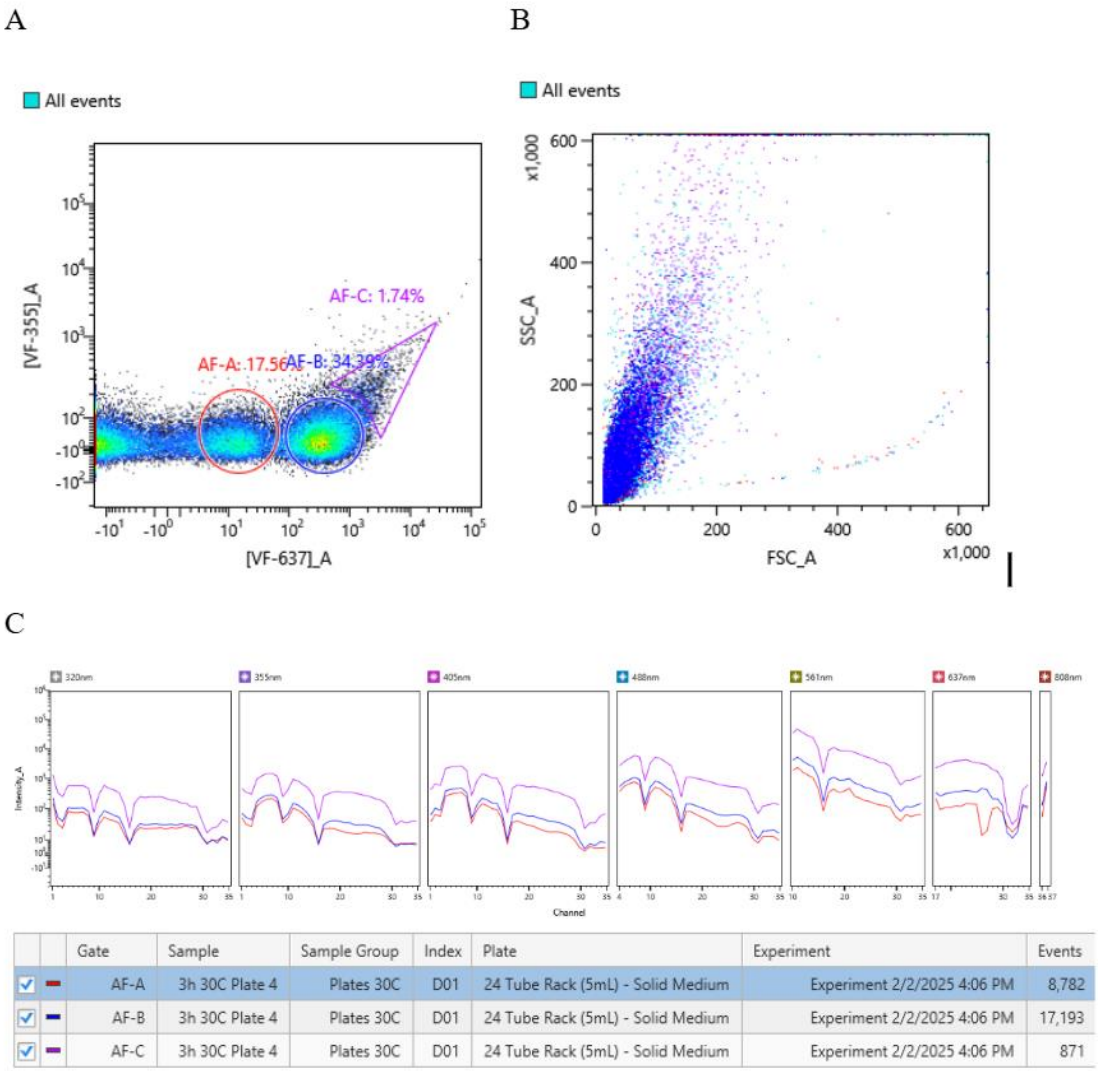

		Gate	Sample	Sample Group	Index	Plate	Experiment	Events
☑	—	AF-A	3h 30C Plate 4	Plates 30C	D01	24 Tube Rack (5mL) - Solid Medium	Experiment 2/2/2025 4:06 PM	8,782
☑	—	AF-B	3h 30C Plate 4	Plates 30C	D01	24 Tube Rack (5mL) - Solid Medium	Experiment 2/2/2025 4:06 PM	17,193
☑	—	AF-C	3h 30C Plate 4	Plates 30C	D01	24 Tube Rack (5mL) - Solid Medium	Experiment 2/2/2025 4:06 PM	871

Figure 5. Autofluorescence signatures of the *S.marcescens* grown for 3 hours on Nutrient Agar at 30 ºC. **A**: Density plot of [VF-355]_A against [VF-637]_A with 3 autofluorescent populations identified. **B**: Scatter plot of the sample (SSC_A against FSC_A). **C**: Overlay plot of the individual populations for each identified autofluorescent population.

A

B

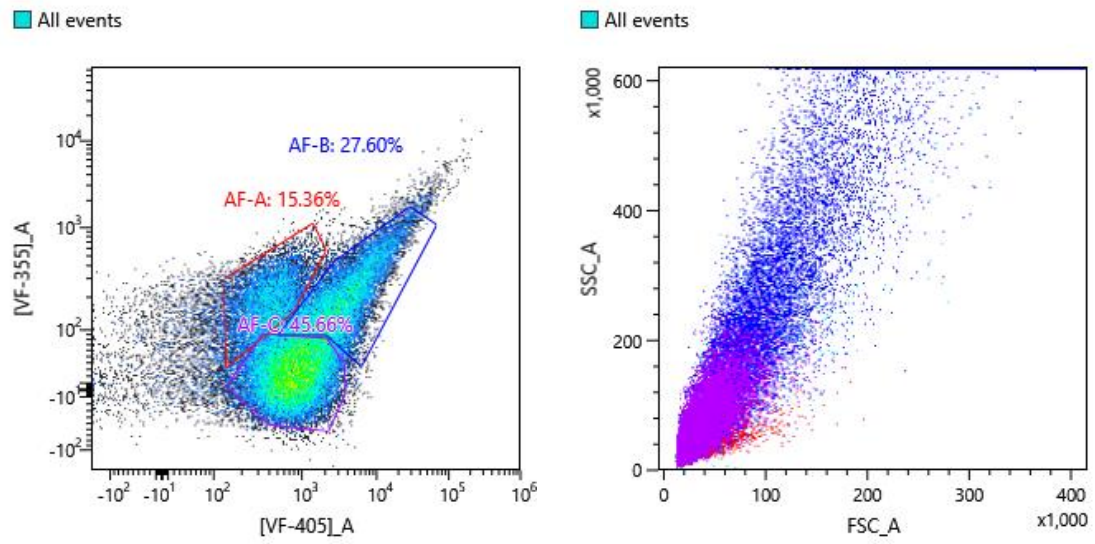

C

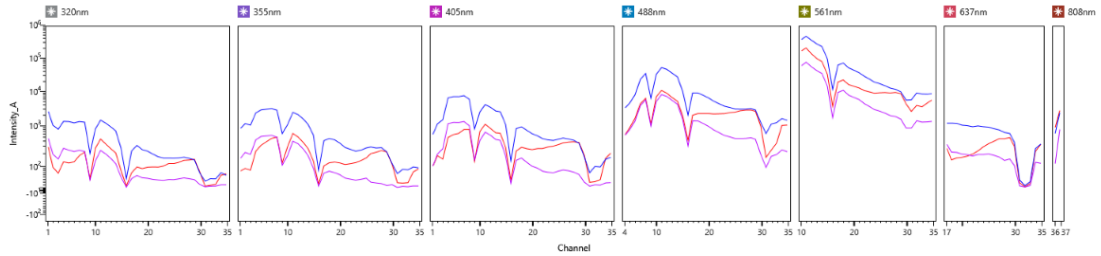

		Gate	Sample	Sample Group	Index	Plate	Experiment	Events
☑		AF-A	9h 30C Plate 4	Plates 30C	D03	24 Tube Rack (5mL) - Solid Medium	Experiment 2/2/2025 4:06 PM	7,679
☑		AF-B	9h 30C Plate 4	Plates 30C	D03	24 Tube Rack (5mL) - Solid Medium	Experiment 2/2/2025 4:06 PM	13,801
☑		AF-C	9h 30C Plate 4	Plates 30C	D03	24 Tube Rack (5mL) - Solid Medium	Experiment 2/2/2025 4:06 PM	22,829

Figure 6. Autofluorescence signatures of the *S.marcescens* grown for 9 hours on Nutrient Agar at 30◦C. **A**: Density plot of [VF-355]_A against [VF-405]_A with 3 autofluorescent populations identified. **B**: Scatter plot of the sample (SSC_A against FSC_A). **C**: Overlay plot of the individual populations for each identified autofluorescent population.

A

B

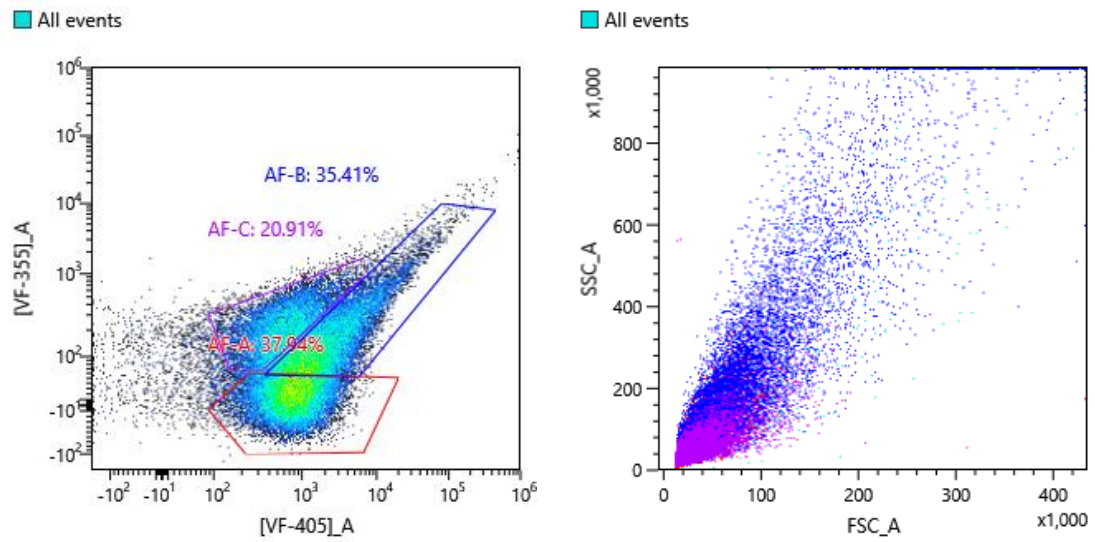

C

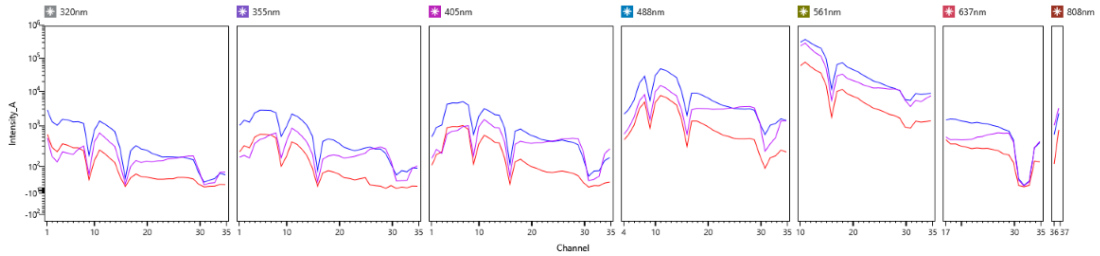

		Gate	Sample	Sample Group	Index	Plate	Experiment	Events
☑		AF-A	12h 30C Plate 4	Plates 30C	D04	24 Tube Rack (5mL) - Solid Medium	Experiment 2/2/2025 4:06 PM	18,968
☑		AF-B	12h 30C Plate 4	Plates 30C	D04	24 Tube Rack (5mL) - Solid Medium	Experiment 2/2/2025 4:06 PM	17,706
☑		AF-C	12h 30C Plate 4	Plates 30C	D04	24 Tube Rack (5mL) - Solid Medium	Experiment 2/2/2025 4:06 PM	10,453

Figure 7. Autofluorescence signatures of the *S.marcescens* grown for 12 hours on Nutrient Agar at 30°C. **A**: Density plot of [VF-355]_A against [VF-405]_A with 3 autofluorescent populations identified. **B**: Scatter plot of the sample (SSC_A against FSC_A). **C**: Overlay plot of the individual subpopulations for each identified autofluorescent population.

A

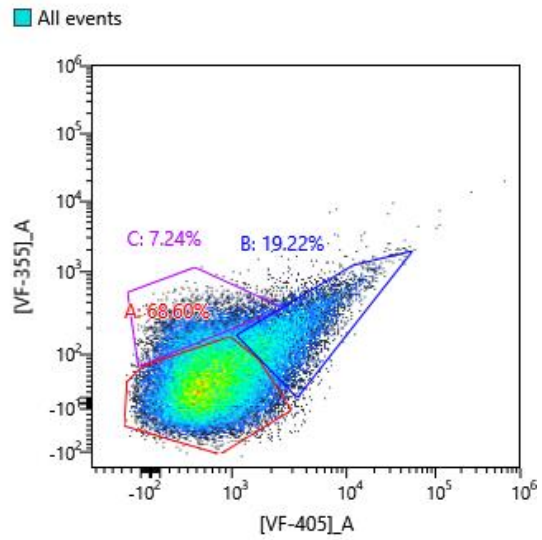

B

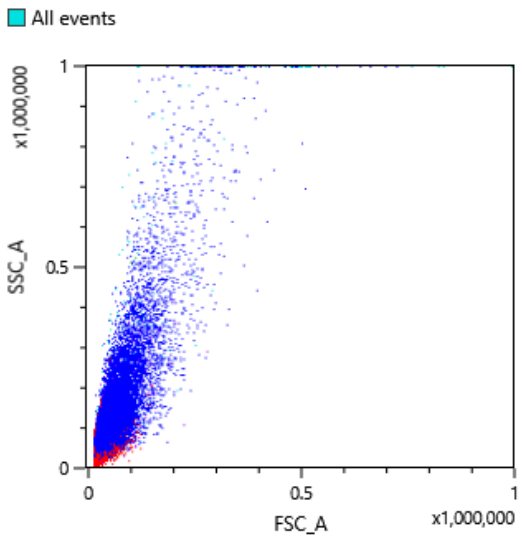

C

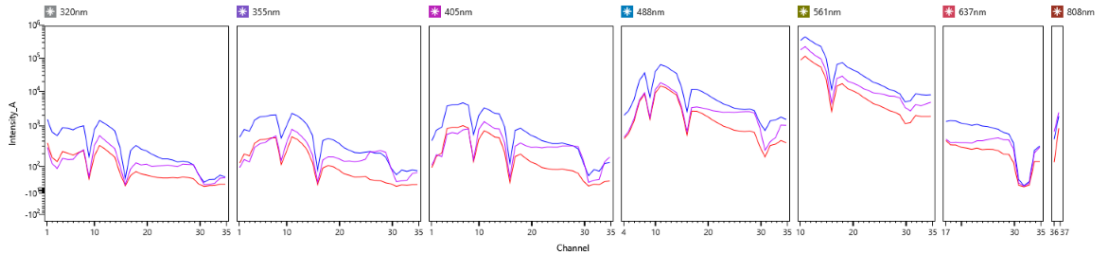

		Gate	Sample	Sample Group	Index	Plate	Experiment	Events
☑		A	15h 30C Plate 1	Plates 30C	A05	24 Tube Rack (5mL) - Solid Medium	Experiment 2/2/2025 4:06 PM	34,300
☑		B	15h 30C Plate 1	Plates 30C	A05	24 Tube Rack (5mL) - Solid Medium	Experiment 2/2/2025 4:06 PM	9,610
☑		C	15h 30C Plate 1	Plates 30C	A05	24 Tube Rack (5mL) - Solid Medium	Experiment 2/2/2025 4:06 PM	3,620

Figure 8. Autofluorescence signatures of the *S.marcescens* grown for 15 hours on Nutrient Agar at 30°C. **A**: Density plot of [VF-355]_A against [VF-405]_A with 3 autofluorescent populations identified. **B**: Scatter plot of the sample (SSC_A against FSC_A). **C**: Overlay plot of the individual subpopulations for each identified autofluorescent population.

4.2.2 Algal full-spectrum analysis

Chlamydomonas reinhardtii

C. reinhardtii generally presents two large event clouds that represent cells with and without autofluorescence, corresponding to chlorophyll autofluorescence signatures.

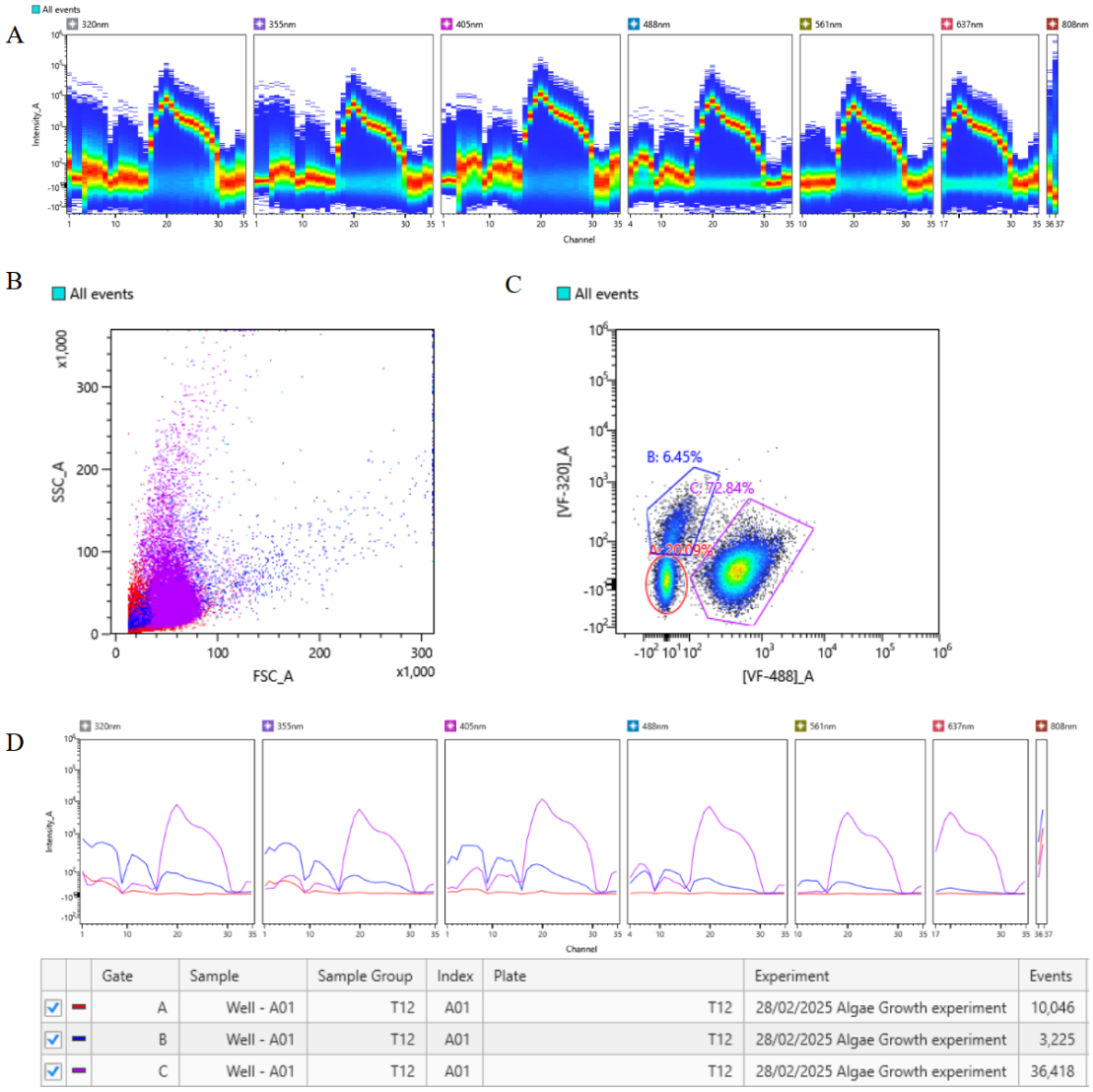

		Gate	Sample	Sample Group	Index	Plate	Experiment	Events
☑		A	Well - A01	T12	A01	T12	28/02/2025 Algae Growth experiment	10,046
☑		B	Well - A01	T12	A01	T12	28/02/2025 Algae Growth experiment	3,225
☑		C	Well - A01	T12	A01	T12	28/02/2025 Algae Growth experiment	36,418

Figure 9. Autofluorescence signatures of the *C.reinhardtii* at the day 12 of growth cycle. **A**: Ribbon plot of the autofluorescence signature of the sample. **B**: Scatter plot of the sample (SSC_A against FSC_A). **C:** Density plot of [VF-320]_A against [VF-488]_A with 3 autofluorescent populations identified. **D**: Overlay plot of the individual subpopulations for each identified autofluorescent population.

The stock sample and sample recorded at T3 (day 3 of growth) are notable exceptions to this pattern. Initial stock samples, represented by the Ribbon Plot below (Figure 10 A), show the presence of a significant number of events that have autofluorescence signature, associated with a low amount of chlorophyll in cells of this phenotype, which is not visible on any other Ribbon plots of other recorded time points. The T3 sample, on the other hand, indicates the presence of two separate phenotypes that have high concentrations of chlorophyll per cell,

marked by both differences in size indicated by discrepancies in the FSC_A/SSC_A density plot and the presence of two separate indications of the Ribbon plot (Figure 11). We can infer that the populations of *C.reinhardtii* loose one of the chlorophyll populations as population enters the growth plateau (Figure 9). During this process the populations starts to increasingly resemble stock population, as autofluorescent non-chlorophyll population increases in proportion and become more visible on the generated density plot (Figure 9 C).

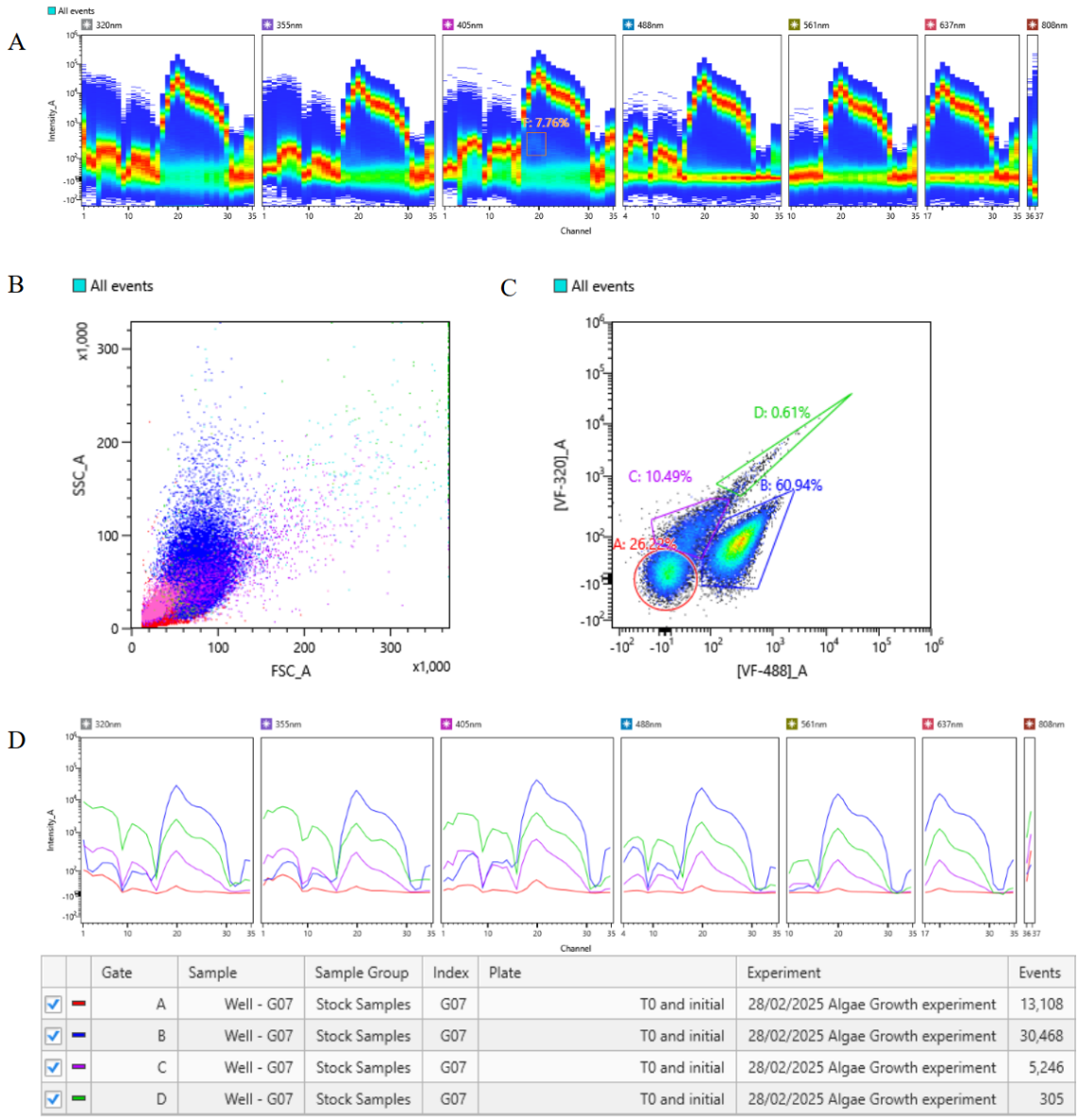

		Gate	Sample	Sample Group	Index	Plate	Experiment	Events
☑		A	Well - G07	Stock Samples	G07	T0 and initial	28/02/2025 Algae Growth experiment	13,108
☑		B	Well - G07	Stock Samples	G07	T0 and initial	28/02/2025 Algae Growth experiment	30,468
☑		C	Well - G07	Stock Samples	G07	T0 and initial	28/02/2025 Algae Growth experiment	5,246
☑		D	Well - G07	Stock Samples	G07	T0 and initial	28/02/2025 Algae Growth experiment	305

Figure 10. Autofluorescence signatures of the initial *C.reinhardtii* sample. **A**: Ribbon plot of the autofluorescence signature of the sample. Gate F present on the Ribbon plot is used to identify the presence of the separately identifiable phenotype. **B**: Scatter plot of the sample (SSC_A against FSC_A). **C:** Density plot of [VF-320]_A against [VF-488]_A

with 4 autofluorescent populations identified. **D**: Overlay plot of the individual populations for each identified autofluorescent subpopulation.

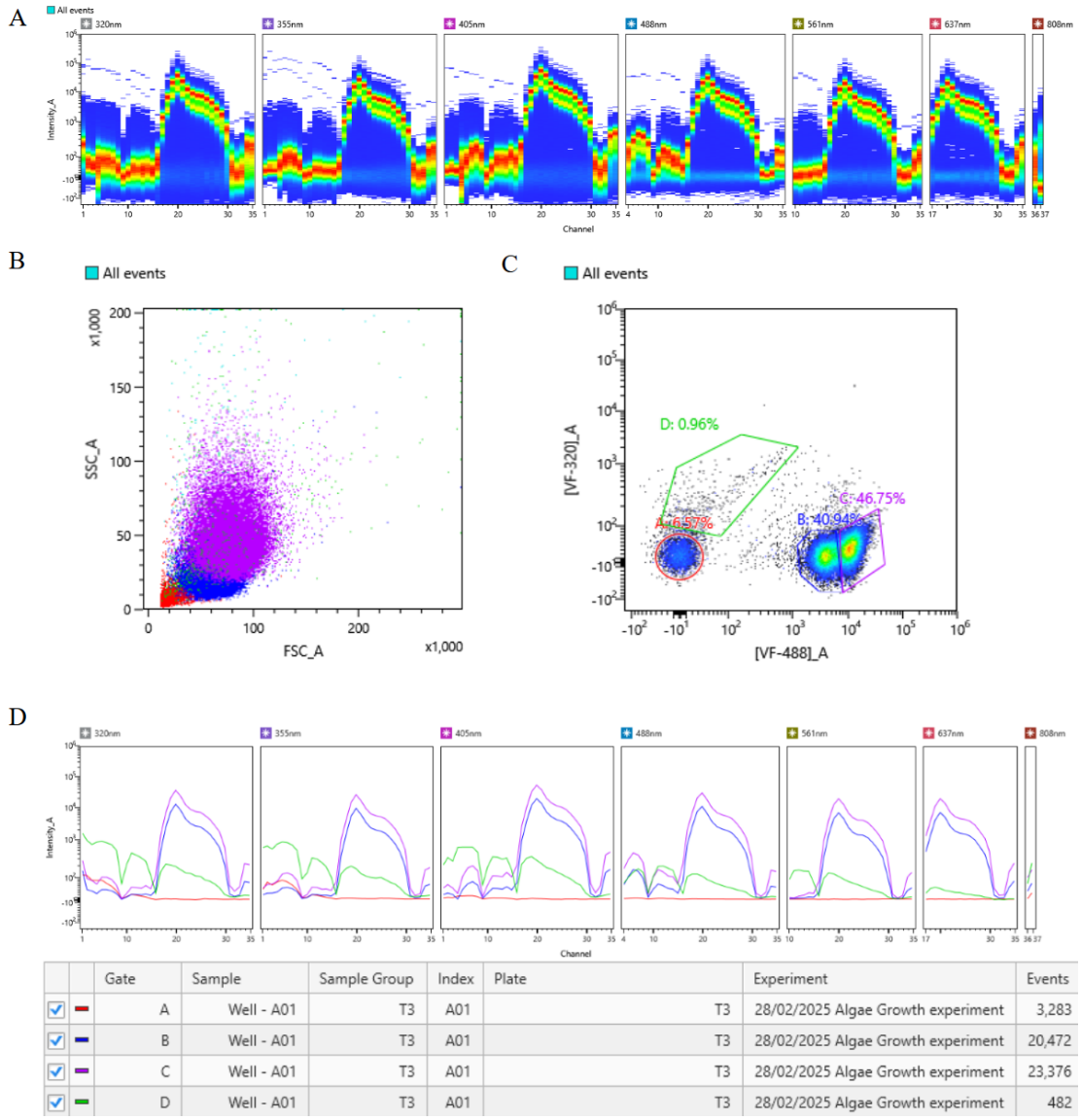

		Gate	Sample	Sample Group	Index	Plate	Experiment	Events
☑		A	Well - A01	T3	A01	T3	28/02/2025 Algae Growth experiment	3,283
☑		B	Well - A01	T3	A01	T3	28/02/2025 Algae Growth experiment	20,472
☑		C	Well - A01	T3	A01	T3	28/02/2025 Algae Growth experiment	23,376
☑		D	Well - A01	T3	A01	T3	28/02/2025 Algae Growth experiment	482

Figure 11. Autofluorescence signatures of the *C.reinhardtii* sample at day 3 of the growth cycle. **A**: Ribbon plot of the autofluorescence signature of the sample. **B**: Scatter plot of the sample (SSC_A against FSC_A). **C:** Density plot of [VF-320]_A against [VF-488]_A with 4 autofluorescent populations identified. **D**: Overlay plot of the individual populations for each identified autofluorescent subpopulation.

Gonium pectorale

Due to its nature as multicellular microscopic algae, *G.pectorale* consistently presents several phenotypes that are easily discernible through both ribbon plots and density plots. Gates that are placed on the FSC_A/SSC_A density plot do not perfectly transpose to the density plots that are created through the autofluorescence finder tool. Due to the overlap in sizes of the phenotypes that exhibit both high- and low-content chlorophyll, gating is preferably done according to the autofluorescence signals. Figure 12 represents the phenotypes present in the *G.pectorale* samples throughout the growth cycle.

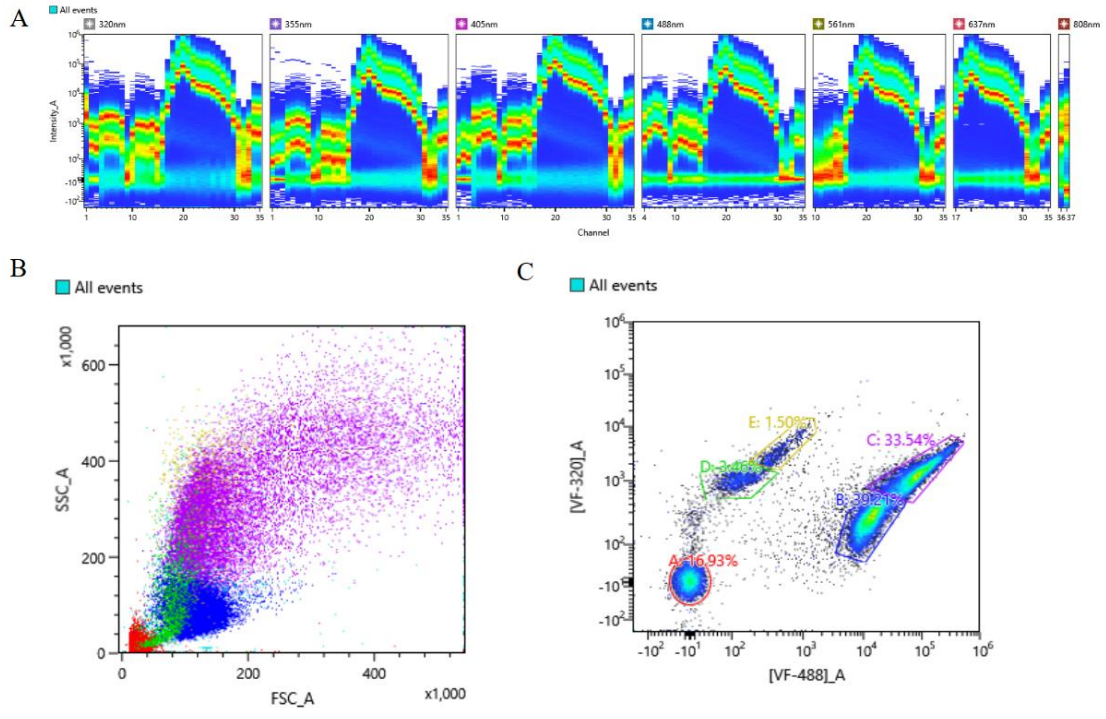

		Gate	Sample	Sample Group	Index	Plate	Experiment	Events
☑		A	Well - A02	T4	A02	T4	28/02/2025 Algae Growth experiment	7,828
☑		B	Well - A02	T4	A02	T4	28/02/2025 Algae Growth experiment	18,136
☑		C	Well - A02	T4	A02	T4	28/02/2025 Algae Growth experiment	15,511
☑		D	Well - A02	T4	A02	T4	28/02/2025 Algae Growth experiment	1,599
☑		E	Well - A02	T4	A02	T4	28/02/2025 Algae Growth experiment	694

Figure 12. Autofluorescence signatures of the *G.pectorale* sample at day 4 of the growth cycle. **A**: Ribbon plot of the autofluorescence signature of the sample. **B**: Scatter plot of the sample (SSC_A against FSC_A). **C:** Density plot of [VF-320]_A against

[VF-488]_A with 5 autofluorescent populations identified. **D**: Overlay plot of the individual populations for each identified autofluorescent subpopulation.

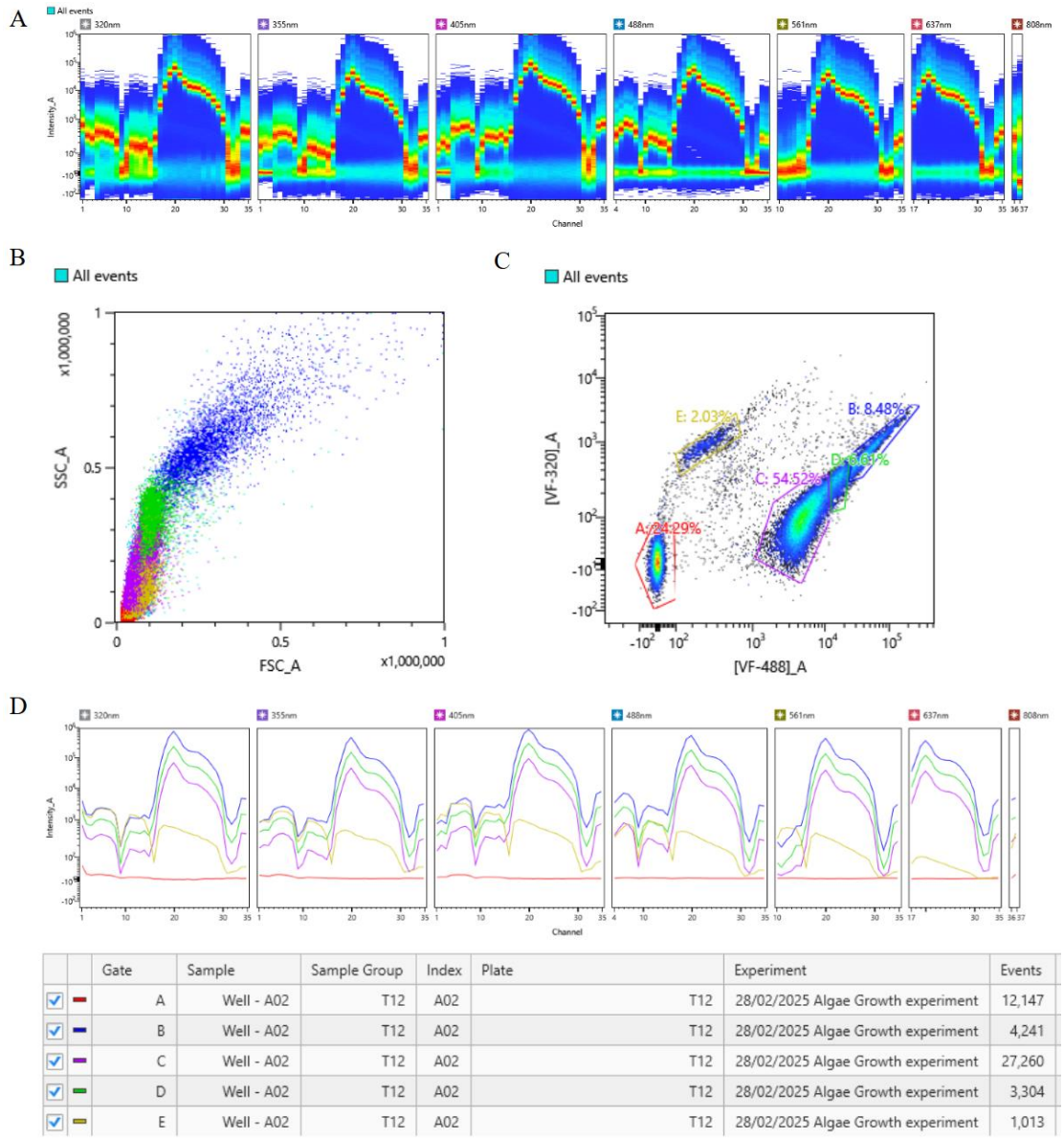

		Gate	Sample	Sample Group	Index	Plate	Experiment	Events
☑		A	Well - A02	T12	A02	T12	28/02/2025 Algae Growth experiment	12,147
☑		B	Well - A02	T12	A02	T12	28/02/2025 Algae Growth experiment	4,241
☑		C	Well - A02	T12	A02	T12	28/02/2025 Algae Growth experiment	27,260
☑		D	Well - A02	T12	A02	T12	28/02/2025 Algae Growth experiment	3,304
☑		E	Well - A02	T12	A02	T12	28/02/2025 Algae Growth experiment	1,013

Figure 13. Autofluorescence signatures of the *G.pectorale* sample at day 12 of the growth cycle. **A**: Ribbon plot of the autofluorescence signature of the sample. **B**: Scatter plot of the sample (SSC_A against FSC_A). **C:** Density plot of [VF-320]_A against [VF-488]_A with 5 autofluorescent populations identified. **D**: Overlay plot of the individual populations for each identified autofluorescent sub population.

Chlorococcum sp.

Chlorococcum, despite being a single-cell organism generates additional phenotypes compared to *C.reinhardtii.* In particular, as seen in Figure 14 A, a multitude of distinct metabolic phenotypes could be observed. Such distinctions are, again, only discernible through emission patterns of the pigments present in the organisms, since alive and dying cells share overlap when analyzed by FSC_A/SSC_A distribution (Figure 14, B).

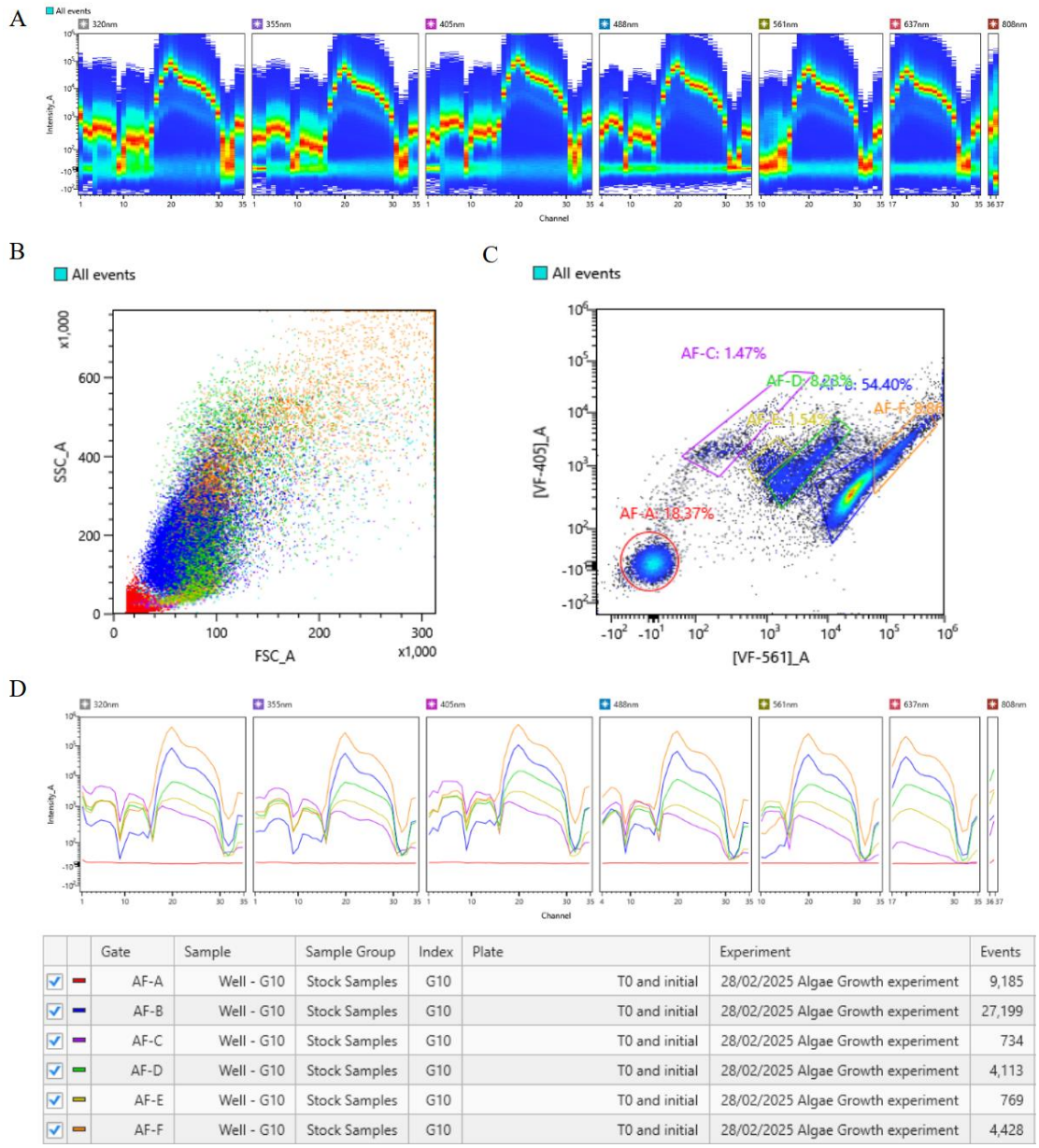

	Gate	Sample	Sample Group	Index	Plate	Experiment	Events
☑	AF-A	Well - G10	Stock Samples	G10	T0 and initial	28/02/2025 Algae Growth experiment	9,185
☑	AF-B	Well - G10	Stock Samples	G10	T0 and initial	28/02/2025 Algae Growth experiment	27,199
☑	AF-C	Well - G10	Stock Samples	G10	T0 and initial	28/02/2025 Algae Growth experiment	734
☑	AF-D	Well - G10	Stock Samples	G10	T0 and initial	28/02/2025 Algae Growth experiment	4,113
☑	AF-E	Well - G10	Stock Samples	G10	T0 and initial	28/02/2025 Algae Growth experiment	769
☑	AF-F	Well - G10	Stock Samples	G10	T0 and initial	28/02/2025 Algae Growth experiment	4,428

Figure 14. Autofluorescence signatures of the initial *Chlorococcum sp.* sample. **A**: Ribbon plot of the autofluorescence signature of the sample. **B**: Scatter plot of the sample (SSC_A against FSC_A). **C:** Density plot of [VF-405]_A against [VF-561]_A

with 5 autofluorescent populations identified. **D**: Overlay plot of the individual populations for each identified autofluorescent subpopulation.

The number of autofluorescent subpopulations fluctuates with the time of the recording within the growth cycle.

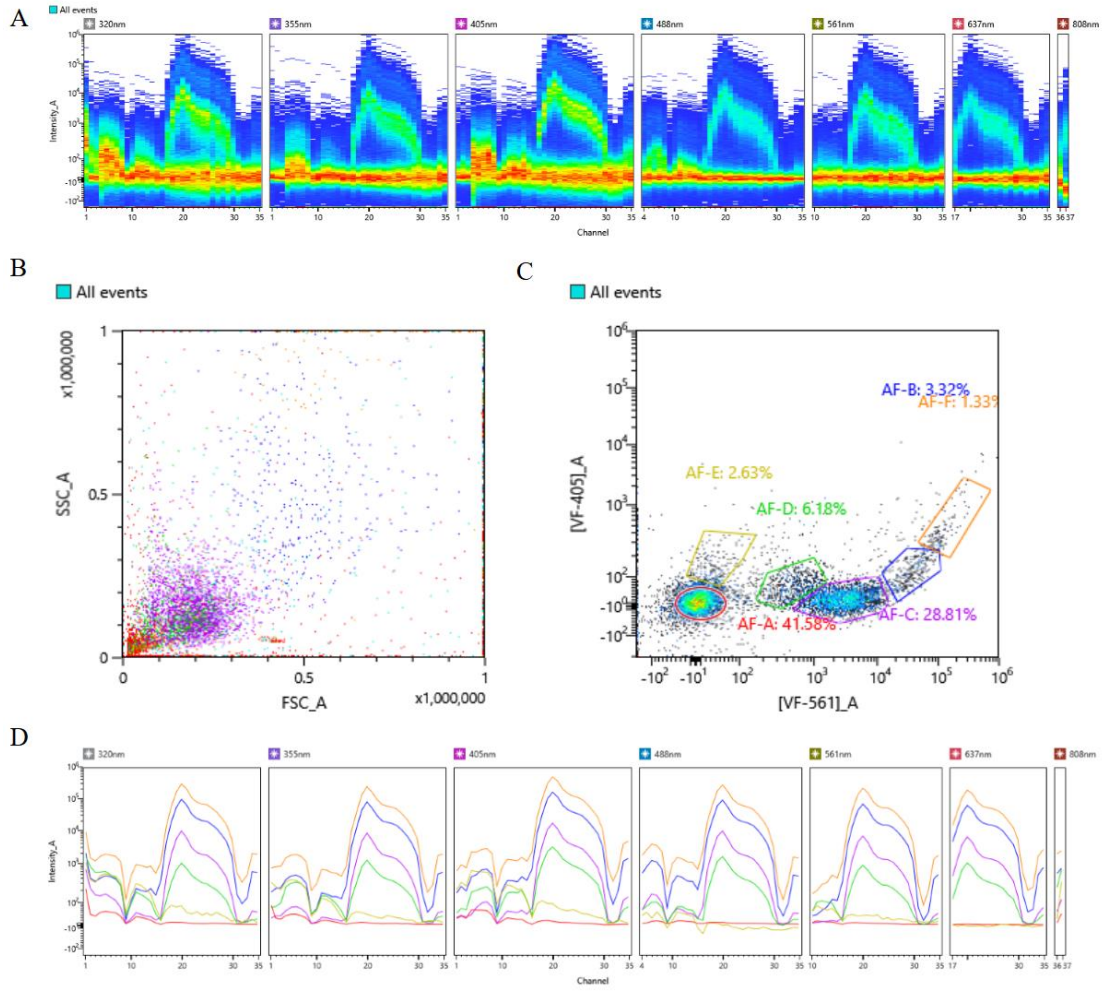

		Gate	Sample	Sample Group	Index	Plate	Experiment	Events
☑		AF-A	Well - F03	T2	F03	T2	28/02/2025 Algae Growth experiment	3,795
☑		AF-B	Well - F03	T2	F03	T2	28/02/2025 Algae Growth experiment	303
☑		AF-C	Well - F03	T2	F03	T2	28/02/2025 Algae Growth experiment	2,629
☑		AF-D	Well - F03	T2	F03	T2	28/02/2025 Algae Growth experiment	564
☑		AF-E	Well - F03	T2	F03	T2	28/02/2025 Algae Growth experiment	240
☑		AF-F	Well - F03	T2	F03	T2	28/02/2025 Algae Growth experiment	121

Figure 15. Autofluorescence signatures of the *Chlorococcum sp.* sample at day 2 of the growth cycle. **A**: Ribbon plot of the autofluorescence signature of the sample. **B**: Scatter plot of the sample (SSC_A against FSC_A). **C:** Density plot of [VF-405]_A against

[VF-561]_A with 6 autofluorescent populations identified. **D**: Overlay plot of the individual populations for each identified autofluorescent subpopulation.

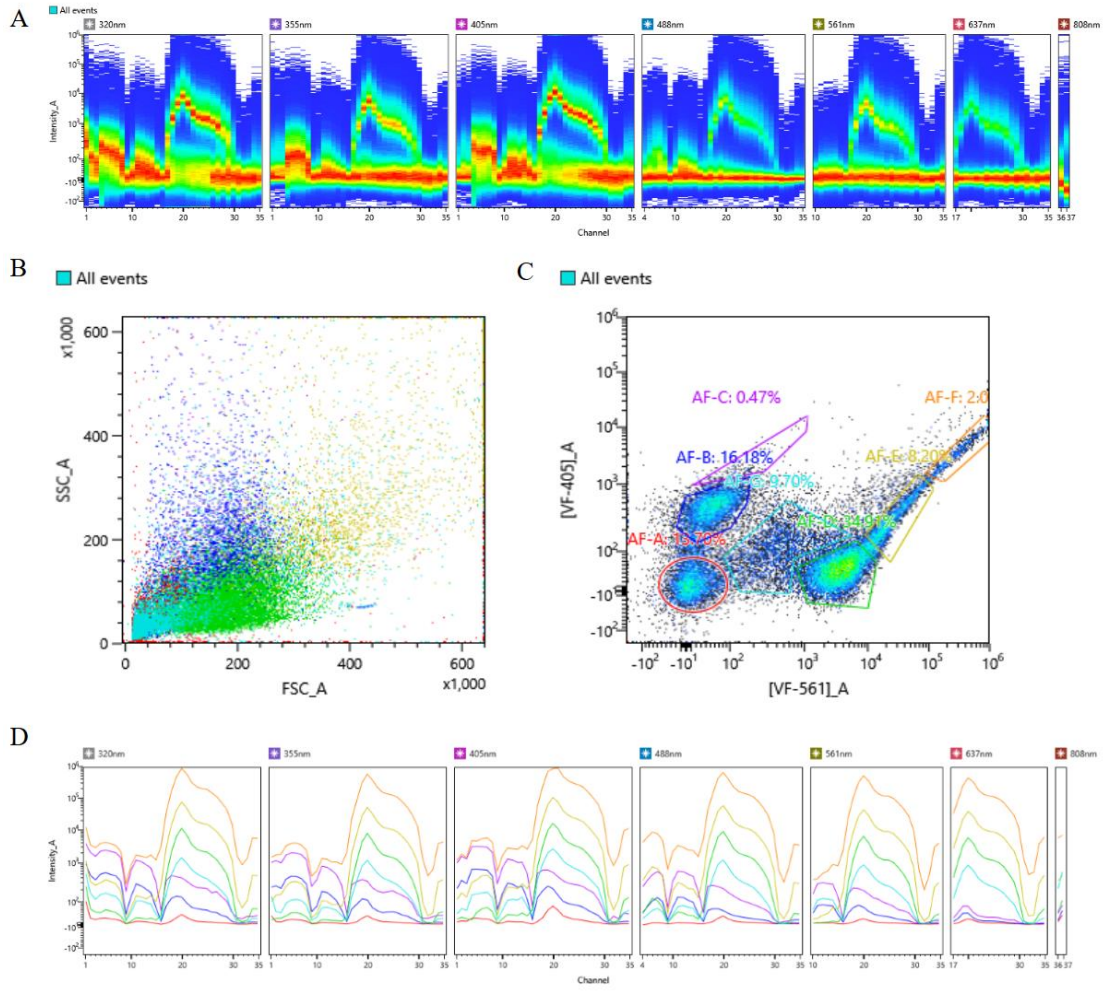

		Gate	Sample	Sample Group	Index	Plate	Experiment	Events
☑		AF-A	Well - A03	T5	A03	T5	28/02/2025 Algae Growth experiment	4,460
☑		AF-B	Well - A03	T5	A03	T5	28/02/2025 Algae Growth experiment	5,267
☑		AF-C	Well - A03	T5	A03	T5	28/02/2025 Algae Growth experiment	152
☑		AF-D	Well - A03	T5	A03	T5	28/02/2025 Algae Growth experiment	11,367
☑		AF-E	Well - A03	T5	A03	T5	28/02/2025 Algae Growth experiment	2,669
☑		AF-F	Well - A03	T5	A03	T5	28/02/2025 Algae Growth experiment	679
☑		AF-G	Well - A03	T5	A03	T5	28/02/2025 Algae Growth experiment	3,157

Figure 16. Autofluorescence signatures of the *Chlorococcum sp.* sample at day 5 of the growth cycle. **A**: Ribbon plot of the autofluorescence signature of the sample. **B**: Scatter plot of the sample (SSC_A against FSC_A). **C:** Density plot of [VF-405]_A against [VF-561]_A with 7 autofluorescent populations identified. **D**: Overlay plot of the individual subpopulations for each identified autofluorescent population.

Pandorina morum

P.morum provides a specific challenge for phenotyping due to its multicellular nature, generating a multitude of phenotypes. As seen on Figure 17A, at least three distinct autofluorescent phenotypes could be determined through the spectral Ribbon plot.

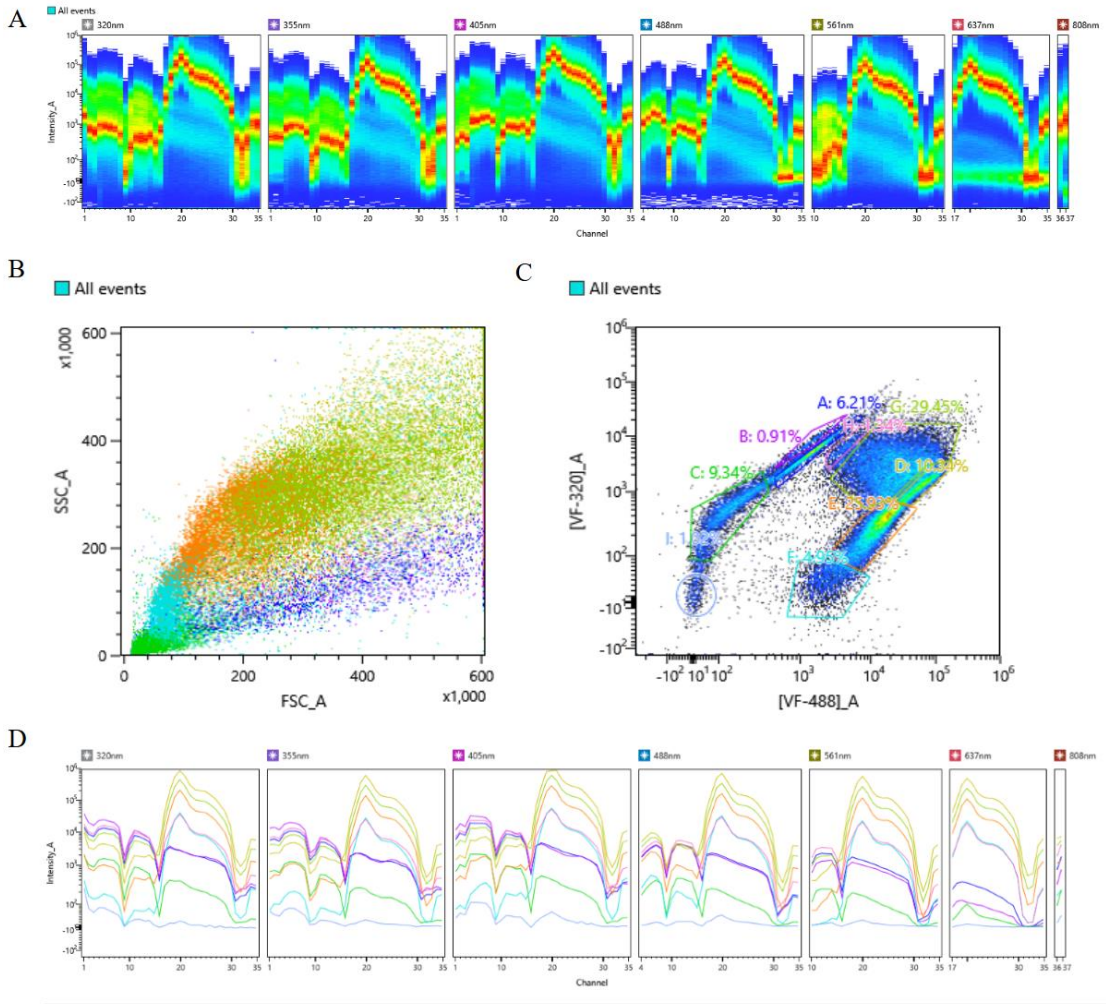

		Gate	Sample	Sample Group	Index	Plate	Experiment	Events
☑	■	A	Well - A04	T12	A04	T12	28/02/2025 Algae Growth experiment	3,104
☑	■	B	Well - A04	T12	A04	T12	28/02/2025 Algae Growth experiment	454
☑	■	C	Well - A04	T12	A04	T12	28/02/2025 Algae Growth experiment	4,671
☑	■	D	Well - A04	T12	A04	T12	28/02/2025 Algae Growth experiment	5,169
☑	■	E	Well - A04	T12	A04	T12	28/02/2025 Algae Growth experiment	12,964
☑	■	F	Well - A04	T12	A04	T12	28/02/2025 Algae Growth experiment	2,477
☑	■	G	Well - A04	T12	A04	T12	28/02/2025 Algae Growth experiment	14,725
☑	■	H	Well - A04	T12	A04	T12	28/02/2025 Algae Growth experiment	670
☑	■	I	Well - A04	T12	A04	T12	28/02/2025 Algae Growth experiment	508

Figure 17. Autofluorescence signatures of the *Chlorococcum sp.* sample at day 12 of the growth cycle. **A**: Ribbon plot of the autofluorescence signature of the sample. **B**: Scatter plot of the sample (SSC_A against FSC_A). **C:** Density plot of [VF-320]_A

against [VF-488]_A with 8 autofluorescent populations identified. **D**: Overlay plot of the individual subpopulations for each identified autofluorescent population.

4.3 Coefficient of Variation (CVs) of Spectra of the Algal Samples

A

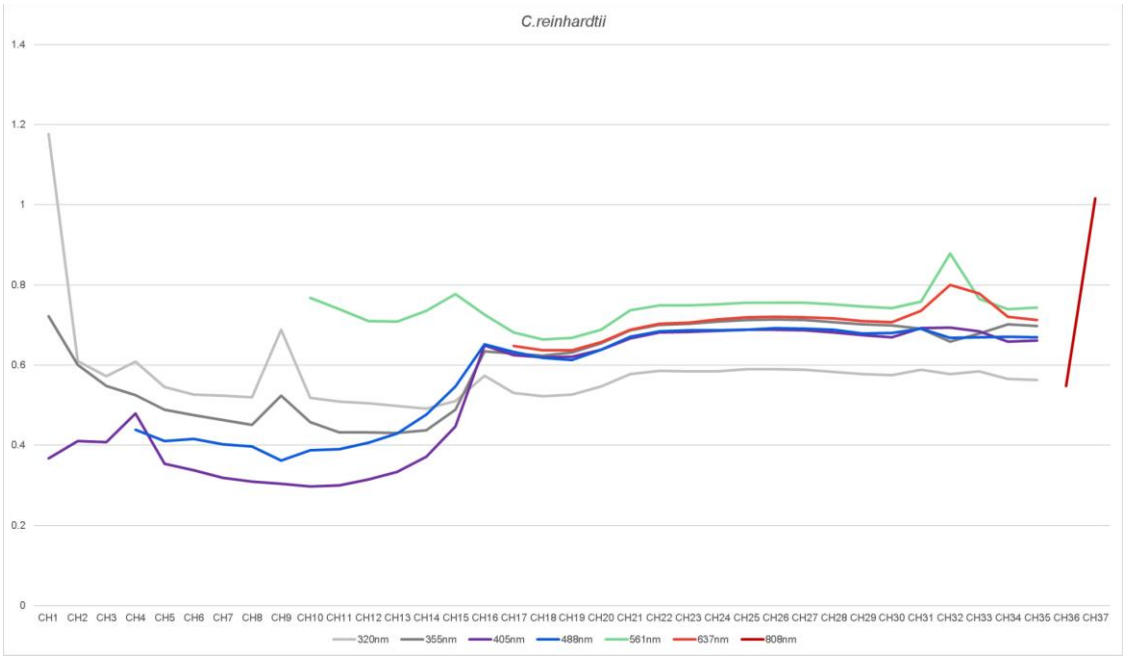

B

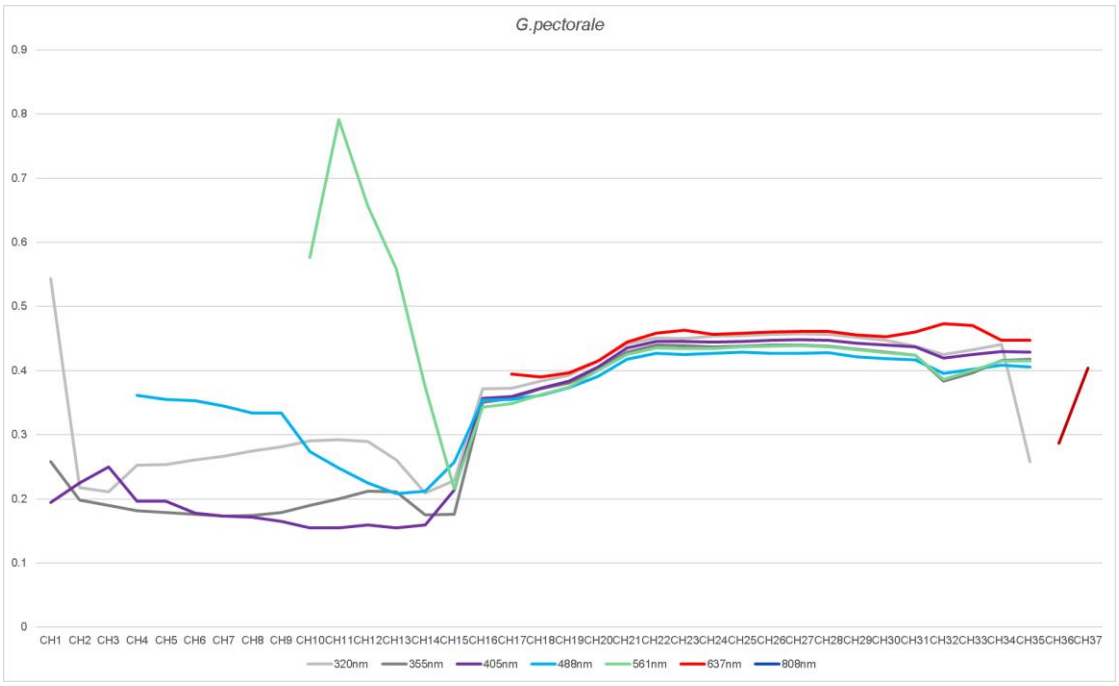

C

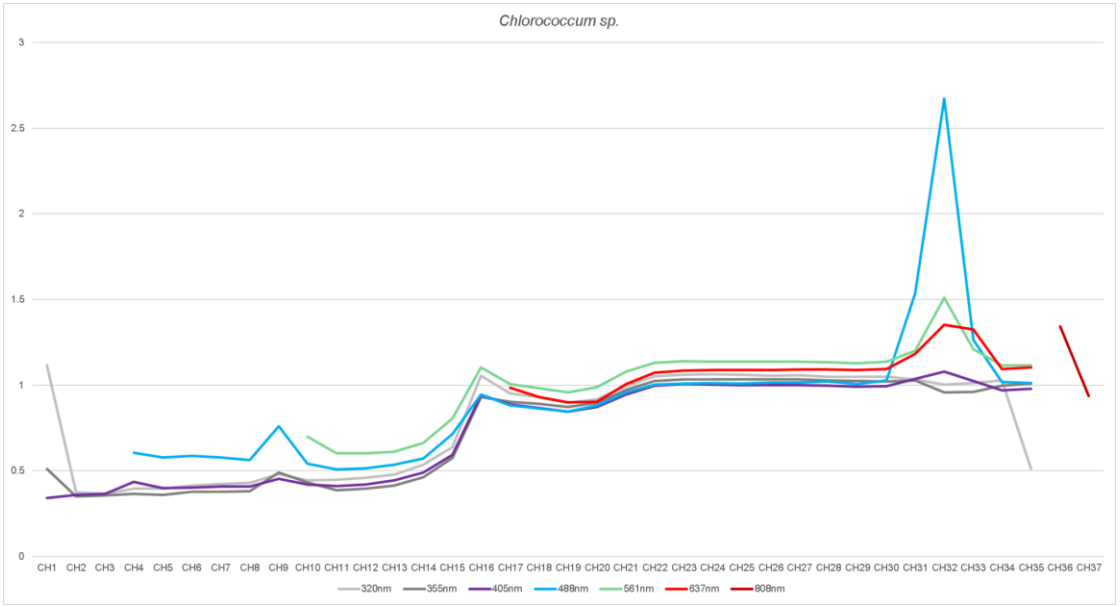

D

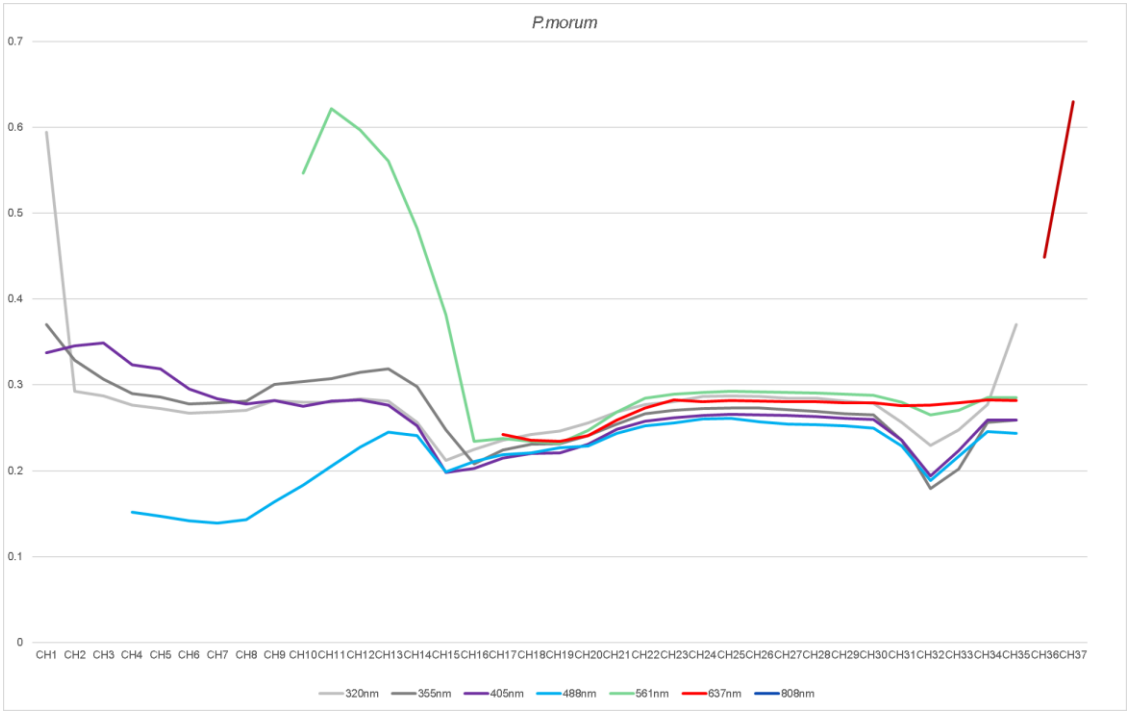

Figure 18. CVs for each of the analyzed organisms. Y-axis represents the value of the CVs for each detection channel shown on the X-axis. Each line represents data for each separate laser. **A:** CVs for *C.reinhardtii* over 12 day growth cycle. **B:** CVs for *G.pectorale* over 12 day growth cycle. **C.** CVs for *Chlorococcum sp.* over 12 day growth cycle. **D.** CVs for the *P.morum* over 12 day growth cycle.

Coefficient of Variation was generated for the overall populations present within the sample, showing the dynamics exhibited within certain wavelengths corresponding to metabolic molecules (CH1 of 320nm laser) and among accessory pigments. Particularly, high variation

of the pigment excitable by 561nm laser that emits in the range of 570-580nm visible light among multicellular *G.pectorale* and *P.morum.* Unicellular *C.reinhardtii* and *Chlorococcum* do not exhibit variation in this region, however they variance in 550-560nm and 815-825nm regions. Additionally, coefficient of variance values are overall higher in unicellular species.

5. Discussion

Analysis of bacterial and algal phenotypes is an important, yet under-discussed area of research, focused mostly on the morphological characteristics of such organisms. Spectral flow cytometry has demonstrated its efficacy in showing the phenotypic diversity of researched species, based on more fundamental characteristics of metabolic properties rather than a well-trodden path of morphological characterization.

The results of this research highlight the advantages of spectral flow cytometry over conventional techniques, specifically in its ability to discriminate between populations based on their autofluorescent parameters.

5.1 Growth Measurements through Optical Density

Recording optical density allows for a fast and convenient recording of the health and growth stages of the microscopic organisms, suspended in liquid media. The recorded data shows that the all samples have undergone stationary, logarithmic and plateau phases of growth, yet have entered them at different times, as was expected from organisms of different life-cycles and biochemistry. Interestingly, all four organisms have entered exponential growth phase around day 3 (T3) and reached their relative ODU peaks around day 10-11-12 (T10, T11 and T12). *C.reinhardtii* and *Chlorococcum sp.* have demonstrated only single peak of the growth cycle, while the *G.pectorale* and *P.morum* have shown two relative peaks, which could be attributed to their multicellular nature and higher number of cells undergoing growth at the time which would correspond to death phase in other organisms.

5.2 Autofluorescence-Based Discrimination of Microbial and Algal Sub-Populations

Spectral flow cytometry demonstrates an exceptional capability to resolve populations of microscopic organisms based on their autofluorescence. Depending on the proportions of the various phenotypes, their presence could be reliably predicted even by the data demonstrated on the spectral ribbon plots. However, many phenotypes that are not present in significant proportion could be found by employing autofluorescence unmixing algorithms.

The advantages of spectral flow cytometry in phenotyping are clearly demonstrated in the case of *S.marcescens*. The presence of at least three phenotypes becomes evident following the color change of the colonies grown on the Nutrient Agar. The peaks that are shown in the “Gate C” of the overlay plot in Figure 6 confirm the clear presence of the prodigiosin pigment. Moreover, the proportion of the different phenotypes could be easily determined based on the number of

events exhibiting the spectral emission parameters associated with the prodigiosin-expressing phenotype.

Similar to the results obtained for the *S.marcescens,* conclusions can be drawn in relation to algal species as well. In particular, time point 3 of the *C.reinhardtii* demonstrates the presence of an additional phenotype that demonstrates a higher emission level, which could be correlated with increased production of the chlorophylls and increased size, compared to other phenotypes present. Most likely, this is a clear demonstration of the presence of the cells undergoing mitosis in a high enough proportion to be easily discernible as a distinct phenotype (supported by FACS-sorting results, not shown).

The advantage of autofluorescence-based phenotyping becomes even more pronounced in the case of multicellular algae *G.pectorale* and *P.morum.* Light scattering data (FSC/SSC) have proven to be insufficient for identifying distinct metabolic phenotypes, especially when these phenotypes are of the same size as chlorophyll-containing cells. Emission-based discrimination not only reveals the presence of phenotypes with high concentrations of metabolically significant molecules but also allows for the monitoring of changes in the proportions of identified phenotypes throughout the growth cycle. *Chlorococcum sp.* is a species that shows the advantages of spectral flow cytometry most prominently. It contains several rare populations that maybe small in proportion, yet exhibit distinct metabolic states specific to the cells of those particular phenotypes. Such populations represent important transitional states of the cells that are easily missed by conventional techniques.

Generally, Optical Density measurements have shown correlation between stage of algae growth and optical density of the sample. The increase of the ODU shows a general increase in the biomass and percentage of healthy organisms, with both assay and spectral flow cytometry showing increase in sample health at the same time.

5.3 Coefficient of Variation of the Algal Samples Spectra

Coefficient of variations results have demonstrated that the changes in the spectral signatures occur in specific regions on the recorded spectra. Particularly all four samples have high CVs numbers in the CH1 of the 320nm laser, which corresponds to the wavelengths reserved for metabolic molecules. All four samples demonstrate similar CVs for the chlorophyll wavelengths, particularly from channels CH18-Ch30. However, unicellular *C.reinhardtii* and *Chlorococcum sp.* have demonstrated high differences in CVs in the CH32-33, which are stable in the multicellular *G.pectorale* and *P.morum.* Latter two in contrast demonstrate high CVs in

the intensities of the CH11 excited by the 561nm laser, which is absent from the unicellular samples. These two peaks are thought to be connected to accessory pigments found in one type of organisms but absent in others. However, demonstrating this connection fully requires further research.

6. Conclusion

As stated in the research question proposed for this project, it is confirmed that metabolic states of cells during growth cycle significantly impact their spectral parameters, and thus lead to the ability to detect algal phenotypes that conventional techniques cannot identify. Spectral Flow Cytometry was able to discriminate microbial and algal subpopulation based on the presence of chlorophyll and accessory pigments, proven to be particularly effective in discriminating populations in multicellular and biofilm-forming algae. Correlations between Optical Density and autofluorescence show correlation between spectral phenotypes and physiological state of the population at the particular point in the growth cycle. Overall, the results of the experiment provide compelling visual evidence that Spectral Flow Cytometry is a robust platform for investigating physiology of microscopic organisms with unprecedented resolution. Such advancements will further refine our ability to monitor, manipulate, and optimize microbial systems for scientific and industrial applications

Despite the insights the research project has provided, several limitations must be acknowledged. First, only a limited number of algal species were utilized with only four species of the same order, limiting the variety of data that may be derived from other species. Secondly, the research was conducted only over a 12-day growth cycle, limiting the applicability of the findings to short-term growth scenarios. Additionally, the analysis of CVs was focused only on the overall changes in the spectral signatures of the species, without distinguishing between individual subpopulations. This may have reduced the precision of the obtained findings.

Further research would require even more sophisticated approaches that would allow to separate each phenotype and research them in greater depth. This could involve integrating Imaging Flow Cytometry to detect distinct morphological phenotypes and linking them to the identified subpopulations. Additionally conducting metabolic assays could help to correlate the presence of certain subpopulations and spectral phenotypes with the metabolic state of the population. Moreover, extending the growth cycle and analyzing individual subpopulations may allow to improve resolution of the CVs of the spectral data, leading to a better understanding of pigment dynamics throughout the growth cycle.

.

7. References

Andreyeva, I.N., Ogorodnikova, T.I. Pigmentation of *Serratia marcescens* and spectral properties of prodigiosin. *Microbiology* 84, 28–33 (2015). https://doi.org/10.1134/S0026261715010026

Barteneva, N. S., Dashkova, V., & Vorobjev, I. (2019). Probing complexity of microalgae mixtures with novel spectral flow cytometry approach and "virtual filtering." https://doi.org/10.1101/516146

Barteneva, N.S. and Vorobjev, I.A., 2023. *Spectral and Imaging Cytometry*. Springer Verlag.

Baker N. R. (2008). Chlorophyll fluorescence: a probe of photosynthesis in vivo. *Annual review of plant biology*, *59*, 89–113. https://doi.org/10.1146/annurev.arplant.59.032607.092759

Behrenfeld, M. J., Westberry, T. K., Boss, E. S., O'Malley, R. T., Siegel, D. A., Wiggert, J. D., Franz, B. A., McClain, C. R., Feldman, G. C., Doney, S. C., Moore, J. K., Dall'Olmo, G., Milligan, A. J., Lima, I., and Mahowald, N.: Satellite-detected fluorescence reveals global physiology of ocean phytoplankton, Biogeosciences, 6, 779–794, https://doi.org/10.5194/bg-6-779-2009, 2009.

Berney, M., et al. (2007). Assessment and interpretation of bacterial viability by using the LIVE/DEAD BacLight Kit in combination with flow cytometry. Applied and Environmental Microbiology, 73(10), 3283-3290.

Berney, M., Hammes, F., Bosshard, F., Weilenmann, H. U., & Egli, T. (2007). Assessment and interpretation of bacterial viability by using the LIVE/DEAD BacLight Kit in combination with flow cytometry. *Applied and environmental microbiology*, *73*(10), 3283–3290. https://doi.org/10.1128/AEM.02750-06

Blair, J., Webber, M., Baylay, A. *et al.* Molecular mechanisms of antibiotic resistance. *Nat Rev Microbiol* 13, 42–51 (2015). https://doi.org/10.1038/nrmicro3380

Croce, A. C., & Bottiroli, G. (2014). Autofluorescence spectroscopy and imaging: a tool for biomedical research and diagnosis. *European journal of histochemistry : EJH*, *58*(4), 2461. https://doi.org/10.4081/ejh.2014.2461

Davey, H. M., & Kell, D. B. (1996). Flow cytometry and cell sorting of heterogeneous microbial populations: the importance of single-cell analyses. *Microbiological reviews*, *60*(4), 641–696. https://doi.org/10.1128/mr.60.4.641-696.1996

Dubelaar, G.B.J., Casotti, R., Tarran, G.A. and Biegala, I.C. (2007). Phytoplankton and their Analysis by Flow Cytometry. In Flow Cytometry with Plant Cells (eds J. Doležel, J. Greilhuber and J. Suda). https://doi.org/10.1002/9783527610921.ch13

Falkowski, P. G., & Raven, J. A. (2013). Aquatic Photosynthesis. Princeton University Press.

Field, C. B., Behrenfeld, M. J., Randerson, J. T., & Falkowski, P. (1998). Primary production of the biosphere: integrating terrestrial and oceanic components. *Science (New York, N.Y.)*, *281*(5374), 237–240. https://doi.org/10.1126/science.281.5374.237

Fierer, N., Leff, J. W., Adams, B. J., Nielsen, U. N., Bates, S. T., Lauber, C. L., Owens, S., Gilbert, J. A., Wall, D. H., & Caporaso, J. G. (2012). Cross-biome metagenomic analyses of soil microbial communities and their functional attributes. *Proceedings of the National Academy of Sciences of the United States of America*, *109*(52), 21390–21395. https://doi.org/10.1073/pnas.1215210110

Georgakoudi, I., Jacobson, B. C., Müller, M. G., Sheets, E. E., Badizadegan, K., Carr-Locke, D. L., Crum, C. P., Boone, C. W., Dasari, R. R., Van Dam, J., & Feld, M. S. (2002). NAD(P)H and collagen as in vivo quantitative fluorescent biomarkers of epithelial precancerous changes. *Cancer research*, *62*(3), 682–687.

Guedes, A. C., Amaro, H. M., & Malcata, F. X. (2011). Microalgae as sources of high added-value compounds--a brief review of recent work. *Biotechnology progress*, *27*(3), 597–613. https://doi.org/10.1002/btpr.575

Harke, M. J., Steffen, M. M., Gobler, C. J., Otten, T. G., Wilhelm, S. W., Wood, S. A., & Paerl, H. W. (2016). A review of the global ecology, genomics, and biogeography of the toxic cyanobacterium, Microcystis spp. *Harmful algae*, *54*, 4–20. https://doi.org/10.1016/j.hal.2015.12.007

Heidelman, M., Dhakal, B., Gikunda, M., Silva, K. P. T., Risal, L., Rodriguez, A. I., Abe, F., & Urayama, P. (2021). Cellular NADH and NADPH Conformation as a Real-Time

Fluorescence-Based Metabolic Indicator under Pressurized Conditions. *Molecules (Basel, Switzerland)*, *26*(16), 5020. https://doi.org/10.3390/molecules26165020

Lakowicz, J. R. (2006). Principles of Fluorescence Spectroscopy. Springer.

Levin-Reisman, I., Ronin, I., Gefen, O., Braniss, I., Shoresh, N., & Balaban, N. Q. (2017). Antibiotic tolerance facilitates the evolution of resistance. *Science (New York, N.Y.)*, *355*(6327), 826–830. https://doi.org/10.1126/science.aaj2191

Marie, D., Brussaard, C. P. D., Thyrhaug, R., Bratbak, G., & Vaulot, D. (1999). Enumeration of marine viruses in culture and natural samples by flow cytometry. *Applied and environmental microbiology*, *65*(1), 45–52. https://doi.org/10.1128/AEM.65.1.45-52.1999

Mukherjee, A., Walker, J., Weyant, K. B., & Schroeder, C. M. (2013). Characterization of flavin-based fluorescent proteins: an emerging class of fluorescent reporters. *PloS one*, *8*(5), e64753. https://doi.org/10.1371/journal.pone.0064753

Nolan, J. P., & Condello, D. (2013). Spectral flow cytometry. *Current protocols in cytometry*, *Chapter 1*, 1.27.1–1.27.13. https://doi.org/10.1002/0471142956.cy0127s63

Paerl, H. W., & Paul, V. J. (2012). Climate change: links to global expansion of harmful cyanobacteria. *Water research*, *46*(5), 1349–1363. https://doi.org/10.1016/j.watres.2011.08.002

Saeys, Y., et al. (2007). A review of feature selection techniques in bioinformatics. Bioinformatics, 23(19), 2507-2517. https://doi.org/10.1093/bioinformatics/btm344

Sosik, H.M., Olson, R.J., Armbrust, E.V. (2010). Flow Cytometry in Phytoplankton Research. In: Suggett, D., Prášil, O., Borowitzka, M. (eds) Chlorophyll a Fluorescence in Aquatic Sciences: Methods and Applications. Developments in Applied Phycology, vol 4. Springer, Dordrecht. https://doi.org/10.1007/978-90-481-9268-7_8

Suller, M. T., & Lloyd, D. (1999). Fluorescence monitoring of antibiotic-induced bacterial damage using flow cytometry. *Cytometry*, *35*(3), 235–241. https://doi.org/10.1002/(sici)1097-0320(19990301)35:3<235::aid-cyto6>3.0.co;2-0